DESIGN OF A LIGHTWEIGHT MODULAR POWERED TRANSFEMORAL PROSTHESIS

A Thesis

by

DANIEL MCGOWAN

Submitted to the Office of Graduate and Professional Studies of
Texas A&M University
in partial fulfillment of the requirements for the degree of

MASTER OF SCIENCE

Chair of Committee,	Pilwon Hur
Committee Members,	Harry Hogan
	Richard Malak
Head of Department,	Andreas A. Polycarpou

May 2017

Major Subject: Mechanical Engineering

ABSTRACT

Rehabilitation options for transfemoral amputees are limited, and no product today can mimic the full functionality of a human limb. Powered prosthetics have potential to close this gap but contain major drawbacks which ultimately increase the energy expenditure of the user. This thesis explores the viability of new designs and methods to reduce energy expenditure. In doing so a prototype containing many of the explored concepts is also being constructed to replace the laboratory's current powered prosthetic, AMPRO II. This goal is accomplished by reducing weight through optimizing structural components, using lightweight motors and gearing, and reducing the energy requirements through novel passive spring sub-assemblies. Adjustable and modular components also enable a wider range of use and are explored. The main objective of this thesis is to investigate these design improvements and create the next-generation prosthetic for the Human Rehabilitation Lab.

This thesis explores using a combination of passive and powered components to reduce the need for heavy actuators. Methods involve coding walking simulations based on an inverse dynamics study. By simulating design concepts with elastic elements the resulting power requirements of the motors have been estimated to evaluate each concept. Motors and gearing options have also been investigated with an optimization-based approach; gearing ratio was minimized in a test comparing discrete off-the-shelf motor options to biomechanical requirements. For the structural components, the mass of each part has been minimized through an iterative approach in FEA.

Elements selected for further investigation from this thesis are being constructed with a prototype. Improvements over AMPRO II include adjustable height, functionality on both legs, a flexible foot, modularity, capabilities of passive elastic elements, and a mass estimated to be 20% lighter. Components include flat motors with harmonic drives, adjustable pylons for height, a low-profile mounting frame, passive pre-loaded springs, and a rotary series elastic actuator (RSEA). Unproven concepts such as the springs and RSEA have been designed as modular and optional to reduce risk. Moving forward, the first prototype is currently being built without the optional components to test the biomechanics. Future tests will incorporate the designed elastic elements to validate simulation concepts.

DEDICATION

I wish to dedicate this work to my wife, Mariel Schottenfeld. Without her patience and support none of this work would have been possible. I thank her for putting up with the years apart needed to complete this work while showing unending love.

ACKNOWLEDGEMENTS

I would like to acknowledge my advisor, Dr. Hur, for his unending support, patience, and guidance. In my time on this work I was able to learn and apply a wide variety of concepts including controls, optimization, design, FEA, and more. I thank Dr. Hur for giving me this opportunity to explore so much with rehabilitation. I also want to thank my committee members, Dr. Hogan and Dr. Malak. Their input was vital to creating a sound design in this multi-disciplinary project. I also extend the acknowledgement to everyone in the Human Rehabilitation (HUR) Group for both making this a fun place to work and also sharing expertise, without which this thesis would not be possible.

NOMENCLATURE

a	Acceleration
COM	Center Of Mass
COP	Center Of Pressure
dx,dy	Distance from points on the Free Body Diagram
E_τ	Percentage off the joint torque value is from the requirement
E_ω	Percentage off the joint speed value is from the requirement
$E_{allowable}$	Maximum allowable error
E_{total}	Summation of error values
FBD	Free Body Diagram
FEA	Finite Element Analysis
F_x, F_y, F_z	Force in stated direction
GR	Gear Ratio
h	Height
I	Moment of inertia
I_{peak1}	Motor current at peak 1 requirement
I_{peak2}	Motor current at peak 2 requirement
K_b	Back EMF Constant
K_t	Torque sensitivity
LSEA	Linear Series Elastic Actuator
m	Mass
M_x, M_y, M_z	Moment in stated direction
p	Position
P	Power
r	Radius of gyration
R	Reaction force, terminal resistance
RSEA	Rotary Series Elastic Actuator
t	Time

T_s	Stall torque
V	Voltage
W_{GR}	Scaling factor for gear ratio
W_τ	Scaling factor for torque
W_ω	Scaling factor for speed
x	COP coordinate
y	COP coordinate
τ	Torque
$\ddot{\theta}$	Angular acceleration
τ_{joint}	Torque at the joint, after the gear ratio
τ_{max_limit}	Maximum torque the motor is capable of
τ_{motor}	Torque at the motor, before the gear ratio
τ_{peak1}	Motor torque at peak 1 requirement
τ_{peak2}	Motor torque at peak 2 requirement
$\tau_{requirement}$	Torque requirement for the joint
ω	Rotational speed
ω_{joint}	Speed at the joint, after the gear ratio
$\omega_{max\_limit}(\tau)$	Maximum speed the motor is capable of, function of torque
ω_{motor}	Speed at the motor, before the gear ratio
ω_n	No load speed
$\omega_{requirement}$	Speed requirement for the joint

Units vary and are clearly stated where needed in this paper.

CONTRIBUTORS AND FUNDING SOURCES

Contributors

This work was supported by a thesis committee consisting of my advisor, Professor Pilwon Hur. Committee members also included Professor Harry Hogan of both the Mechanical Engineering and Biomedical Engineering departments and Professor Richard Malak of the Mechanical Engineering Department.

The work conducted for this thesis was completed by the student independently.

Funding Sources

Graduate study was supported by a Graduate Research Assistantship from Professor Pilwon Hur's startup funding and by a Graduate Teaching Assistantship also from Mechanical Engineering at Texas A&M University.

TABLE OF CONTENTS

Page

ABSTRACT ii

DEDICATION iv

ACKNOWLEDGEMENTS v

NOMENCLATURE vi

CONTRIBUTORS AND FUNDING SOURCES viii

TABLE OF CONTENTS ix

LIST OF FIGURES xi

LIST OF TABLES xv

1. INTRODUCTION 1

1.1. Importance and Literature Review 1
1.2. Example Devices 5
1.3. Research Goals 7

2. INVERSE DYNAMICS ANALYSIS 10

2.1. Experiment and Calculations 10
2.2. Calculated Results & Requirements for Prosthetic 15

3. COMPONENT DESIGN AND SIMULATIONS 18

3.1. Design Goals & Assembly 18
3.2. Motors and Gearing 20
3.2.1. Methods 20
3.2.2. Optimization 24
3.2.3. Optimization Results 31
3.3. Elastic Elements and Walking Simulations 33
3.4. Ankle Springs 39
3.4.1. Ankle Spring Physical Design 42
3.5. Rotary Series Elastic Actuator 43
3.5.1. RSEA Results 46
3.5.2. RSEA Physical Spring Design 47
3.5.3. RSEA Assembly Design 49
3.6. Ankle Joint Modular Options 50

3.6.1. Rigid Ankle Joint Option 50
3.6.2. Changing Components 50
3.7. Height & Leg Adjustment 51

4. GEOMETRY AND STRUCTURAL DESIGN 54

4.1. Model Setup 54
4.1.1. Simplifications 54
4.1.2. Interface Conditions 55
4.1.3. FEA Design Method 56
4.2. Upper Frame FEA 57
4.2.1. Loading and Boundary Conditions 57
4.2.2. Meshing 58
4.2.3. Load Cases 59
4.2.4. Results & Convergence 61
4.3. Bottom Frame 64
4.3.1. Loading and Boundary Conditions 64
4.3.2. Meshing 65
4.3.3. Load Cases 66
4.3.4. Results & Convergence 67
4.4. RSEA 70
4.4.1. Loading and Boundary Conditions 70
4.4.2. Meshing 71
4.4.3. Load Cases 72
4.4.4. Results 72
4.4.5. Convergence 78

5. HARDWARE, MANUFACTURING, AND ASSEMBLY 81

6. RESULTS 83

6.1. Final Device Design 83
6.2. Future Work 85
6.3. Impact of Thesis 86

7. CONCLUSIONS 87

REFERENCES 89

APPENDIX A: MOTOR OPTIONS 93

APPENDIX B: FEA DETAILS 95

APPENDIX C: PROTOTYPE DRAWINGS 103

LIST OF FIGURES

Page

Figure 1. Example RSEA Spring Designs from Phall et al.[17] 4

Figure 2. Example Powered Prosthetics. Texas A&M [26], Vanderbilt [19] 6

Figure 3. AMPRO II, Texas A&M, 2016 7

Figure 4. Marker Positions Plot 11

Figure 5. Link Segment Model FBD 14

Figure 6. Joint Angles (Left) and Moments (Right) 16

Figure 7. Joint Power (Left) and Work (Right) 16

Figure 8. Human Joint Data 17

Figure 9. Example Motor Curve (moog.com) [33] 21

Figure 10. Peak Moment and Speed at Ankle 23

Figure 11. Example Plot of Motor Operating Points 24

Figure 12. Motor Optimizer Constraint Check 25

Figure 13. Failed Gearbox Design Concept 30

Figure 14. Optimizer Attempt to Reach Worst Case Values 31

Figure 15. Captured Ankle Torque from Human Data 32

Figure 16. Example Walking Simulation of Elastic Elements 34

Figure 17. LSEA Angle Impact 35

Figure 18. Power Required from Motor Based on Spring Stiffness for LSEA 36

Figure 19. Power Values from LSEA Simulation 37

Figure 20. Toe Springs Simulation 38

Figure 21. Preloaded Ankle Spring Simulation 39

Figure 22. Ankle Spring Moment Calculations 40

Figure 23. MATLAB Walking Simulation 42
Figure 24. Modular Ankle Spring Components 43
Figure 25. RSEA Deflection 44
Figure 26. Torsional RSEA Optimized for Power 46
Figure 27. RSEA Design Generation Shape 1 48
Figure 28. RSEA Design Generation Shape 2 48
Figure 29. RSEA Assembly 49
Figure 30. Rigid Ankle Joint Mount 50
Figure 31. Ankle Joint Elastic Options 51
Figure 32. Adjustable Pylon & Belt Tensioner 52
Figure 33. FEA Geometry Simplification 55
Figure 34. FEA Connections/Interface Conditions 56
Figure 35. Example FEA Design Iteration (Plotting SF) 57
Figure 36. Upper Frame Loads and Boundary Conditions 58
Figure 37. Mesh of Upper Structural Components 59
Figure 38. Ground Reaction Force Profile 60
Figure 39. Main Frame Mount FEA, von-Mises Stress 62
Figure 40. Upper Frame Knee Bracket FEA 63
Figure 41. Fatigue SF of Upper Frame 64
Figure 42. Bottom Frame Loads and Boundary Conditions 65
Figure 43. Mesh for Ankle Bracket Structural Parts 66
Figure 44. Ankle Load Case 1 FEA Results 67
Figure 45. Lower Frame von-Mises Stress, Static Analysis 68
Figure 46. Stress Singularity at Corner 69

Figure 47. Ankle Bracket Fatigue Safety Factor 69
Figure 48. RSEA Spring Disk Loads and B.C. 71
Figure 49. RSEA Mesh 71
Figure 50. RSEA Results for Perpendicular Loop Concept 73
Figure 51. RSEA Spring Disk Concept – Three Parellel Loops 74
Figure 52. Elastic-Plastic Results Showing No Plastic Deformation 74
Figure 53. Elastic-Plastic Analysis Stress Results 75
Figure 54. RSEA Disk - Four Parallel Loops 76
Figure 55. Final RSEA Disk Stress 77
Figure 56. Final RSEA Disk Deflection 77
Figure 57. RSEA Connecting Disk FEA Results 78
Figure 58. RSEA Mesh Convergence Study 79
Figure 59. Mesh Convergence 80
Figure 60. Ankle Design Exploded View 82
Figure 61. Upper Frame Exploded View 82
Figure 62. Proposed Device 84
Figure 63. Prosthetic Part Diagram 85
Figure 64. Operating Points for Maxon 429271 94
Figure 65. Mesh for Simplified Connection Parts 95
Figure 66. Ankle Interface Conditions 1 96
Figure 67. Ankle Interface Conditions 2 96
Figure 68. Frictional Interface on Ankle Bracket 97
Figure 69. Top Frame Iteration 1 Results 98
Figure 70. Top Frame Iteration 2 Results 98

Figure 71. Top Frame Iteration 3 Results 99
Figure 72. Top Frame Iteration 4 Results 99
Figure 73. Bottom Frame Iteration 1 Results 100
Figure 74. Bottom Frame Iteration 2 Results 100
Figure 75. Bottom Frame Iteration 3 Results 101
Figure 76. Bottom Frame Iteration 4 Results 101
Figure 77. Bottom Frame Iteration 5 Results 101
Figure 78. Ankle Link 1 103
Figure 79. Ankle Link 2 103
Figure 80. Top Knee.....104
Figure 81. Top Mount 104

LIST OF TABLES

Page

Table 1. Schedule of Continued Project Work.....86

Table 2. Motor Options.....93

1. INTRODUCTION

1.1. IMPORTANCE AND LITERATURE REVIEW

Amputations impact the lives of a significant portion of the world's population today. Many people require some type of rehabilitation for mobility and living happy lives. In the United States, lower extremity amputations occur at a rate of approximately 185,000 people per year [1]. It also takes up to 60% more metabolic energy compared to healthy subjects for transfemoral amputees to walk [2]. Even though many rehabilitation and treatment options exist, no product today can mimic the full functionality of a human limb. With that in mind, the intent of this thesis is to develop the next generation powered lower limb prosthetic at Texas A&M. Recent advancements in research and technology of rehabilitation robotics have been investigated and applied to the design to create an improved prosthetic both for rehabilitation and research purposes.

Powered prosthetics have potential to close the gap between passive prosthetics and healthy limbs. They are a new technology in comparison to the conventional passive prosthetic devices and require more research to be viable for most users. Currently only one powered ankle and one powered knee, the Ossür power knee, are on the market [3]. The major drawbacks of the technology include cost, lack of functionality, mass, and bulky designs. Mass and bulk, for example, significantly increase the energy expenditure of the users and can negate the benefits of a powered device. Such drawbacks are further discussed by researchers [4, 5]. Other powered prosthetic devices exist in research labs

but are currently only being used for research purposes and have not solved many of the issues around the technology.

For proper imitation of able-bodied limbs, prosthetic devices must be able to mimic functionality, speeds, and torques of healthy humans with minimal weight and volume. To determine these requirements, kinematic and kinetic joint data have been calculated using inverse dynamics. Studies have shown joint torque and speed can be estimated based on the weight of the user using this method [6]. Taking into account a user of 200lbs and the worst case ranges by such studies, the ankle joint must be capable of producing 172Nm of torque while the knee joint must be capable of 90Nm. More recent studies also give additional insight into the energy profile requirements for lower limb prosthetics such as power and work expectations for prosthetics [7]. The prosthetic design in this thesis is developed to meet these requirements. New data for these requirements have also been gathered with details explained in the methods section.

The high torque requirements are a major contributing factor to the high weight of powered lower limb prosthetics. In order to generate the required power, heavy motors with large gearing systems could be employed. However, meeting the power requirements solely through motors and gearing is not viable due to the mass and resulting footprint of motors that are capable of generating such a torque. Alternatively, other methods must be provided to produce and store the required power. Many studies have also stated the importance of improving efficiency of the prosthetics [8-11]. Rather than removing the motors and returning to fully passive devices, many studies today are looking into methods to reduce the required power of the motors by mixing both passive

and powered components; doing so will allow less bulky and lighter-weight prosthetics, reducing energy expenditure of the user. A researcher investigating the power and work of foot structures concluded elastic energy storage and return has potential to replicate the profiles of healthy limbs [7]. One such successful use of elastic energy storage is through the use of a Linear Series Elastic Actuator (LSEA). The use of a LSEA for a robotic tendon has been developed by Hollander et al. [9] and has shown great potential at reducing energy requirements to power a prosthetic. This concept consists of a linear actuator and spring in series which provide a torque to the ankle by pushing down on a moment arm secured to the ankle joint. The series elastic tendon is reported to reduce peak power requirements for the ankle from 250 W to 77 W. Due to its advantages, a LSEA has been employed by other researchers that also reported enhanced energy consumption on their devices, such as a clutchable knee device [12, 13]. Cherelle et al. also installed a spring on the foot which gathers energy from an ankle dorsiflexion and has also reported an enhancement in energy consumption [14].

Another popular mechanism in prosthetics is a Rotary Series Elastic Actuator (RSEA). These devices can be used for torque control, shock tolerance, energy storage, and to reduce stiffness between the device and the user [15, 16]. A RSEA is similar to a LSEA in that it consists of a deflecting spring in series with an actuator. In contrast, however, the spring is designed as a torsion spring machined from a flat disk. Rather than relying on linear motion and requiring a moment arm to generate the joint torque, the spring is in line with the motor shaft keeping the energy rotational. On prosthetics these devices are normally used for improved torque control rather than reducing power

requirements. The deflection of the spring is measured and with a known spring constant the torque can be calculated, as shown by successful tests in labs [17]. An example of spring design concepts from literature is shown below, from Phallen et al.

Figure 1. Example RSEA Spring Designs from Phall et al.[17]

In an effort to counteract the high mass of traditional powered devices, applying soft robotics to prosthetics has also been gaining some momentum in research labs. One study used dielectric elastomer actuators which consist of lightweight materials that change stiffness based on an applied voltage [18]. The idea behind this is to replace heavy metallic parts with soft lightweight materials and by controlling the voltage researchers can force motions. Unfortunately, the study concluded that the technology holds promise but is not yet feasible for use in prosthetic devices (the study focused on upper limb but the conclusions still hold for other prosthetics). The major issue holding it back appears to be researchers being unable to increase stiffness to a level useful for use in a prosthetic. The technology does seem viable if further improvements are made and more studies are likely to continue in the coming years. The use of soft robotics also holds promise to adjust stiffness values on series elastic actuators used in lower limb prosthetics.

1.2. EXAMPLE DEVICES

Functional powered lower limb prosthetics today aim at mimicking able-bodied limbs, but they do not all use the same methods. There is a growing trend, however, of taking advantage of springs (such as was discussed with the LSEA) as a means to reduce energy requirements. The AMP Foot 2.0 [14] was able to closely follow the joint torque and power curves of an ankle during the walking (gait) cycle. The device uses a LSEA but is however, still undesirably bulky and heavy. Other devices use more simplified approaches and consist only of some motors and gearing on a single frame. These can be lighter weight due to fewer components, but due to the high power and torque requirements previously discussed, such devices are usually only capable of flat-foot walking. Flat-foot walking is unnatural and undesirable due to increased energy expenditure [4]. Examples of existing powered prosthetics are presented in the following figure from Texas A&M (AMPRO I) and the Center for Intelligent Mechatronics [19]. The Vanderbilt design is one of the only few with a pylon for height adjustment. It should be noted that the pylon needs to be swapped out for another of different length and is not itself adjustable. The Vanderbilt design also separated the electronics for the ankle and knee and secured parts in close proximity to the joints, while the AMPRO I has all of the actuator components placed in the center of the calf. Other powered prosthetics from research institutions have also been investigated and share similar design concepts with variations including elastic elements and actuators [12, 20-23].

AMPRO I (Texas A&M)

Center for Intelligent Mechatronics

Figure 2. Example Powered Prosthetics. Texas A&M [26], Vanderbilt [19]

The most recent powered prosthetic from Texas A&M (excluding that proposed in this thesis) is the AMPRO II. The device consists of a single aluminum frame with two brushless DC motors and harmonic drives for gearing. A single frame supports the user and components as shown in Figure 3. Timing belts connect the actuators to the joints for motion. The device is battery powered with a belt strap used to hold the battery on the user and away from the prosthetic. The foot is flat with no flexibility and the prosthetic is designed for flat foot walking as opposed to multi-contact. Several control methods for this prosthetic were developed [24-26]. A study investigating the performance of AMPRO II identified several factors for improvement [4]. The study found the importance of kinetic and kinematic gait symmetry (joint angles, angular velocity, and reaction forces).

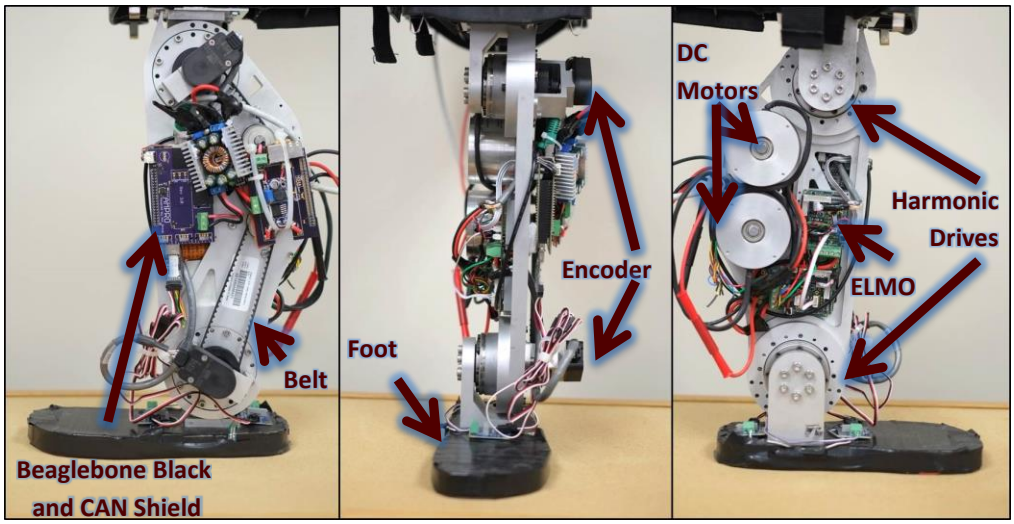

Figure 3. AMPRO II, Texas A&M, 2016

Moving forward, there is a clear need for improvement. Prosthetics today do not come close to mimicking the full functionality of healthy limbs. Powered devices have potential to provide the missing functionality but quickly become unrealistic with the required complexity and added mass of powered components and ultimately may increase the energy expenditure of the user rather than decrease it over passive devices. To move forward, researchers must develop new methods to provide the functionality while focusing on reducing mass and volume as key factors. In doing so, the device should also maintain gait symmetry [4].

1.3. Research Goals

The high level goal of this research is to produce the next generation above-the-knee prosthetic for the Human Rehabilitation Group at Texas A&M. Based on literature reviews and needs of the lab, several improvements are to be made aimed at (1) reducing

the energy expenditure of the user, (2) accommodating a larger range of users, and (3) creating a device capable of testing future research concepts (AMPRO II is only capable of use on one leg and at a single height with flat-foot walking, which limits potential research). Mass is considered a key design factor in part selection. Motors and gearing make up the heaviest components of the device; the motors and gearing systems have thus been selected based on an optimization based approach. Structural components contribute as the second heaviest components and as such material volume reduction is another goal. To be useful for both a multitude of users and research experiments, modularity is also a key component. Unlike existing powered prosthetics, this device should be adjustable for users of different heights or on either leg.

To ensure the device is useful for rehabilitation and not just laboratory testing, unproven concepts are planned to be modular components. For example, one area of potential is the addition of elastic elements for energy saving purposes. Keeping these elastic elements as optional and removable springs will satisfy this requirement. The modularity of such components also allows easy adjustment for the needs of different users and easy testing of the new concepts. Modularity also allows specific components to be upgraded in the future without the need of redesigning the entire device. A flexible off-the-shelf foot is planned for the initial prototype and for this thesis but can be upgraded to a custom foot later, for example.

The focus of the thesis is on the mechanical aspects of the design. As such, electronics and controller designs are out-of-scope. With proper modifications, existing electronics and controller concepts from AMPRO II can be applied to the new device in

the future. Human testing of the prosthetic is also out-of-scope for this thesis but planned as future work. Several modular components are being developed and a successful design will be capable of employing all of proposed modular components for future use. For example, some initial design concepts have been developed for optional components such as ankle-springs and a RSEA. These concepts are presented and are proposed in theoretical simulations (MATLAB/inverse dynamics) but are not planned for the initial prototype build. As such, finalized physical designs for these optional components are not part of this thesis and are planned as add-ons for future work. Though a physical prototype is being built, since component build times may vary and are uncontrollable the project focus is based on the design, analysis, and simulations.

2. INVERSE DYNAMICS ANALYSIS

2.1. EXPERIMENT AND CALCULATIONS

The requirements were gathered using inverse dynamics and a link-segment model. Data were both gathered from published data and through experiments. Items of interest from the data were the joint reaction forces, net muscle moments, power, and work in the lower extremity. For the experiment, a single healthy male volunteer has been used and kinematic data has been captured with a passive marker motion capture system (at 100Hz) and kinetic data by a Bertec Corporation force plate (at 1000Hz) using the motion capture lab at Texas A&M. Sample rates have been chosen to satisfy the Nyquist criteria. Raw data output was an analog voltage. Raw data contained force plate output signals that have been converted into forces and moments in accordance with the procedures provided by Bertec Corporation. Raw position data consisted of position data for each marker. The coordinate systems of the data did not all match so values have been converted into a global coordinate system (GCS). Makers were placed at the heel, toe, ankle, knee, hip, shoulder, and back. Precise positioning of markers closely matching published studies [27, 28] which can be referenced along with Figure 4 for more placement details. All data analysis was computed using MATLAB. Data was collected as the volunteer walked normally while stepping his right foot once on the force plate.

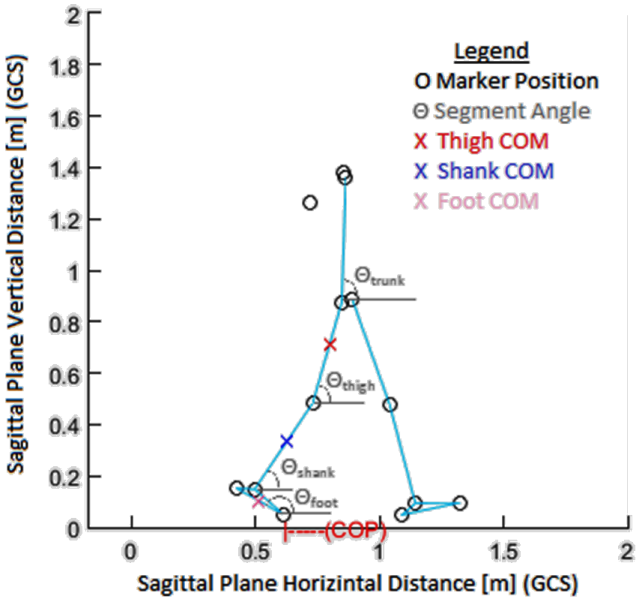

Figure 4. Marker Positions Plot

Processing the data started by subtracting the baseline analog voltage from all signals to bring the signal bases to zero. Next, data was filtered using a 2nd order Butterworth filter with a cutoff frequency of 5Hz for marker data and 10Hz for force plate data. To prevent aliasing and line up the data sets, force plate data has been down sampled to 100Hz after filtering. Force platform data was then used to calculate the ground reaction forces (GRF) and moments through the procedures outlined by the Bertec Corporation manual. The center of pressure (COP) has been calculated as:

$$x = \frac{-hF_x - M_y}{F_z}, \; y = \frac{-hF_y - M_x}{F_z} \qquad (1)$$

The coordinates of the COP are x and y, h is the thickness of material on top of the force plate (.0032m for the cover), F is the force in the directions stated by subscripts

and M is the moment in the direction stated by subscripts. To prevent errors in calculations, all F_z values below 10lbf have been neglected. After calculations, the GRF and COP have been converted the global coordinate system.

Gait speed was calculated as the distance the marker on the right shoulder moved in the sagittal plane over time. Step length was calculated as the distance between the left and right heel in the sagittal plane. The time between consecutive steps was calculated and averaged over several steps to get the cadence, which is steps per minute. An example output of the positions of the markers, COM, and COP, which were used for calculations, is shown in Figure 4.

Segment angle and joint angles were calculated for one complete gait using the right lower extremity only (shown on the left in Figure 4) from the point of heel contact on the force plate to the next heel contact on the ground. Segment angles are shown in Figure 4, which were used to calculate joint angles. Plantar flexion, knee extension, and hip extension are considered positive. Joint angular velocities have been calculated as the change in angle divided by time for each time step. Angular acceleration was calculated using Equation 3, where 'a' is the acceleration, 'i' each time step, 'p' is the position (angle) at the indicated time step, and 't' is the time between time steps. Linear acceleration was calculated using the same equation but with 'p' representing the linear distance rather than angle.

$$a_i = \frac{p_{i+1} - 2p_i + p_{i-1}}{\Delta t^2} \qquad (2)$$

Anthropometry data from Leva (1996) has been used for several calculations. The volunteer's weight is 158lbf. Following the instructions and tables provided by Leva (1996), that weight has been used to calculate the mass of each segment. The COM location and radius of gyration were also obtained with those tables. Segment lengths have been obtained by calculating the distance between markers shown in Figure 4. Moment of inertia was then calculated for each segment using Equation 3.

$$I = mr^2 \qquad (3)$$

An inverse dynamics analysis has been performed to determine net muscle moments and joint reaction forces. Each segment of the right lower extremity (foot, shank, and thigh) has been represented by a link segment model. A free body diagram (FBD) of a link is shown in the following figure. The same FBD applies to each segment, with joint 1 being the joint under the segment of interest and joint 2 being above. For the foot, the forces at joint 1 are from the ground reaction force (which was calculated as explained above).

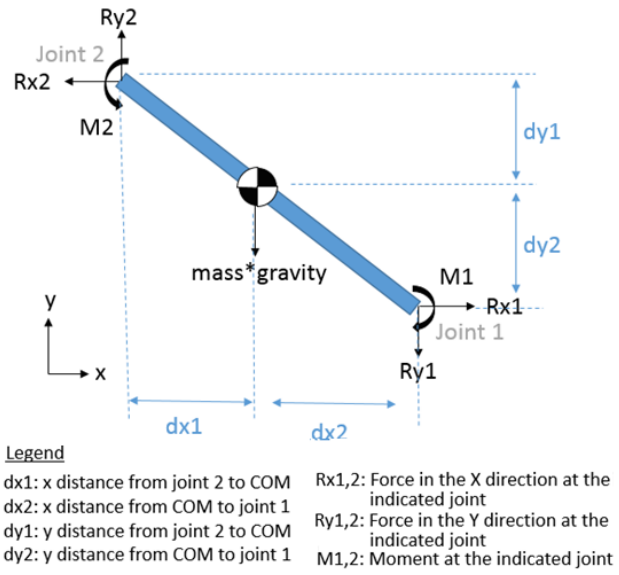

Figure 5. Link Segment Model FBD

Analyzing the FBD provides the following resultant equations, where 'm' represents the mass of the segment, 'a' is the linear acceleration in the indicated direction, 'I' is moment of inertia and '$\ddot{\theta}$' is the angular acceleration.

$$\sum F_x = R_{x1} - R_{x2} = ma_x \qquad (4)$$
$$\rightarrow R_{x2} = -(ma_x - R_{x1}) \qquad (5)$$

$$\sum F_y = R_{y2} - R_{y1} - mg = ma_y \qquad (6)$$
$$\rightarrow R_{y2} = ma_y + R_{y1} + mg \qquad (7)$$

$$\sum M_{COM} = -R_{y2} * dx1 + R_{x2} * dy1 + M2 + R_{x1} * dy2 - R_{y1} * dx2 - M1 = I\ddot{\theta} \qquad (8)$$
$$\rightarrow M1 = -R_{y2} * dx1 + R_{x2} * dy1 + M2 + R_{x1} * dy2 - R_{y1} * dx2 - I\ddot{\theta} \qquad (9)$$

The equations above have been used to solve for the moments at each joint. Joint power and joint work have also been calculated. The power is the product of angular

acceleration and the moment. Joint work is the integral of the power curve with respect to time. The experiment and calculations have been computed using two walking speeds, a normal speed and hurried. Plots are shown in the following section. The methods and experimental results have been compared to publications and gave similar results [4, 6, 29-31].

To account for potential ranges in values from variation in people, plots of an expected range of values for torque in the knee and ankle are also calculated. Results are shown in Figure 8 are based on a 200lb user. These values have been calculated based on weight impacts predicted by Winter [32].

2.2. Calculated Results & Requirements for Prosthetic

Results from the inverse dynamics analysis through experimental data are plotted next. Joint angles for the hip, ankle, and knee are plotted for the hurried and normal trials. Note that the 100% Gait Cycle is 1.11 seconds for the normal trial and 0.93 seconds for the hurried trial. Moments are plotted with knee extension, hip extension, and plantar flexion positive.

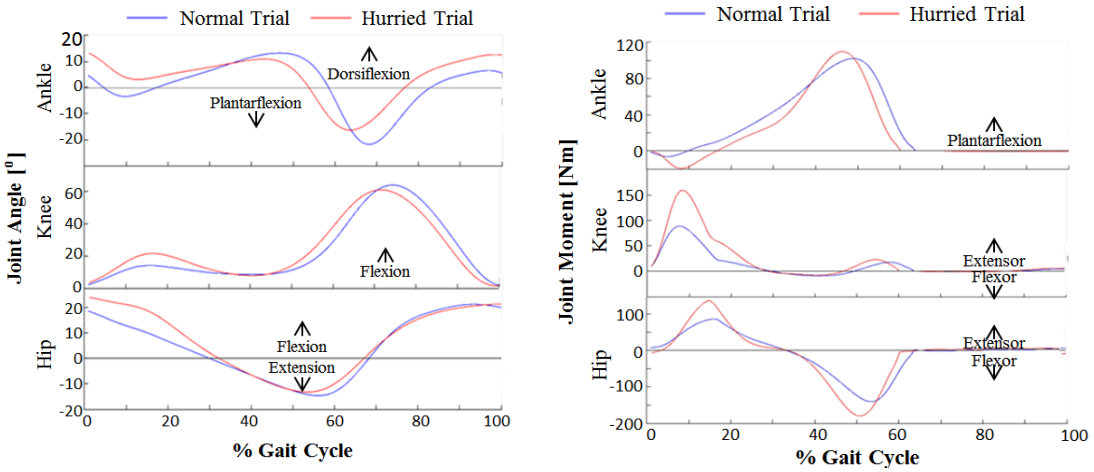

Figure 6. Joint Angles (Left) and Moments (Right)

Joint power and joint work are compared in Figure 7 below.

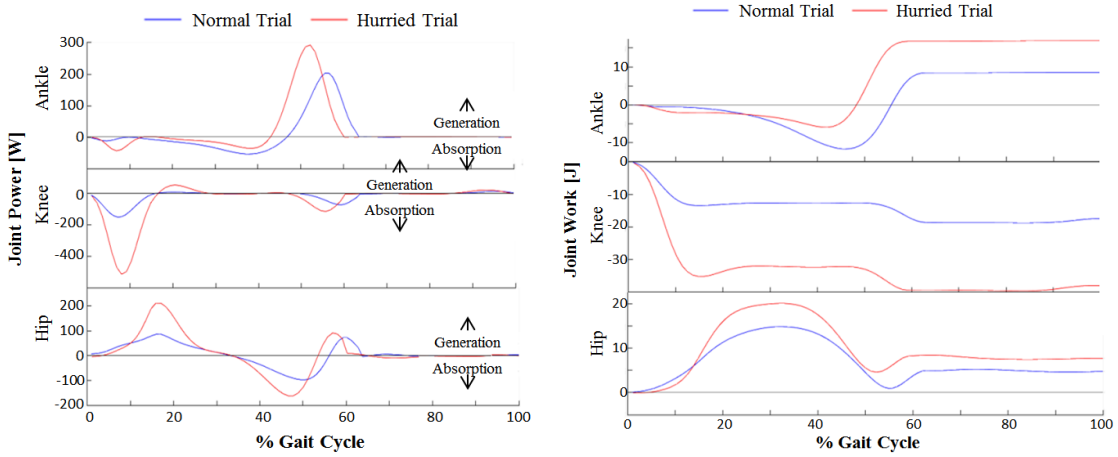

Figure 7. Joint Power (Left) and Work (Right)

The methods and experimental results have been compared to publications and gave similar results [4, 6, 29-31]. As discussed, data has also been compared to published data and plots created to take into account variation for users up to 200lbs based on weight impacts predicted by Winter [32]. These results are plotted in Figure 8.

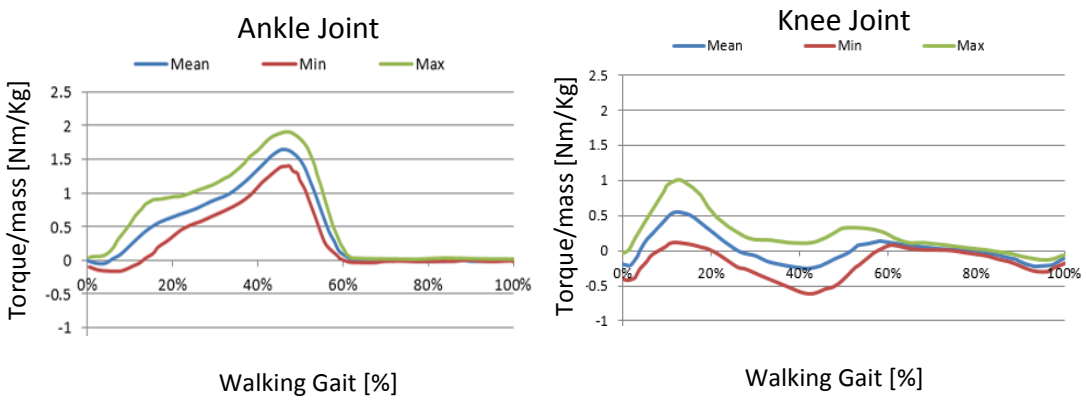

Figure 8. Human Joint Data

3. COMPONENT DESIGN AND SIMULATIONS

3.1. DESIGN GOALS & ASSEMBLY

From the research goals discussed in Chapter 1, the intent of this thesis is to design a prosthetic device that will reduce the energy expenditure of the user, accommodate a larger range of users, and create a device more useful for research in the laboratory. The following design constraints have been applied to accommodate the goals:

- Modular
    - It is impossible to make a single device that is perfect for everyone. Customization required for different patients is a major cause of the high costs of prosthetics. Keeping modularity in mind while designing components is important as it helps reduce this problem by allowing adjustments on the device without expensive intervention by engineers or doctors. This device is also to be used in a research lab and creating a product capable of interchanging components for various purposes vastly increases the potential of research in the lab.
- Heavy components and electronics placed close together and as close to the residual limb as possible
    - This is aimed mainly at the motors and gearing. Placing them near the residual limb aids in modularity as each part of the device can be designed in sub-sections and interchanged. This also reduces strain on the

user as the heavy components will create less of a moment arm during a leg swing if they are closer to the residual limb.

- Adjustable Length
    - Various methods have been investigated for adjusting height. To aid in modularity, a pylon was chosen. The pylon itself is described in the results and is self-adjustable, which is unique to these devices.
- Minimized Weight
    - High mass is one of the major causes of increased energy expenditure of the user [4]. Keeping that in mind, components have been selected in an attempt to minimize the weight, such as motors and gearing. Structural components are also minimized through FEA analysis.
- Elastic Components
    - As discovered through the analysis of motors and gearing in this thesis, it is impossible to reach all extreme points with a single motor and gearing option. Creating something capable of the high end of values also significantly adds mass and bulk to the design. That being said, it was considered important to investigate passive elastic components as a lighter weight means of storing and providing some of the power during walking. This is similar to human limbs in that healthy limbs also have elastic components, such as the Achilles tendon.

Component selection is also based on off-the-shelf parts when possible to reduce cost. A frame has been designed as described through FEA with an optimized motor and gearing system, which is described in Chapter 4. Several components have also been chosen for modularity and adjustability. Modular components, such as the elastic elements, are not being constructed with the initial prototype but to be continued in future work. A summary of the proposed device is shown in the results, Figure 62.

3.2. Motors and Gearing

3.2.1. Methods

Actuators must be chosen to meet the requirements from Figure 8. To do so, motor and gearing selecting is based on an optimization approach. Discrete data points have been created from off-the-shelf motor options. Motors considered are shown in Appendix A. An important note from Figure 8 is the largest torque is not applied to the knee or ankle joint during the entire gait cycle. With that in mind, motors can theoretically safely run past the advertised continuous values without overheating. An example of running past the continuous use value is the intermittent value shown from Moog [33] in Figure 9. Intermittent values have been estimated based on input and plots from the manufacturer. To the best knowledge of the author, other prosthetics are not designed with these intermittent values in mind. This is important for finding optimum motors as using the intermittent specifications allows use of much smaller and lighter weight motors. These values are determined based on a maximum temperature rise with the typical allowable rise on commercial motors being 75˚C [34].

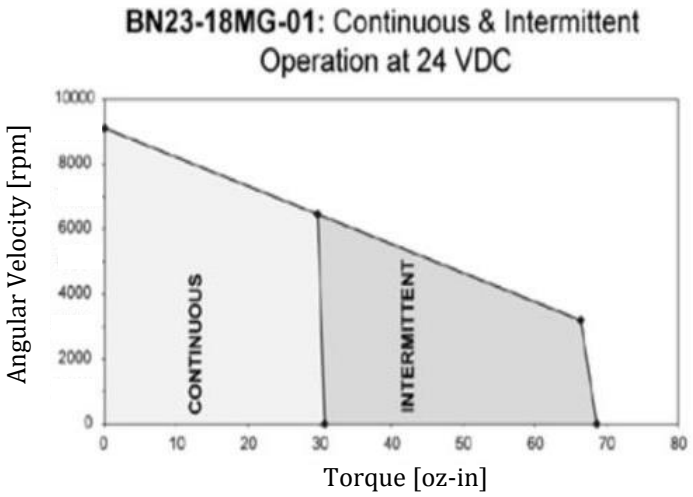

Figure 9. Example Motor Curve (moog.com) [33]

Calculation of current, power, speed, and voltage vary based on the source and motor manufacturer. For this thesis, motor operating calculations have been computed based on standard methods from machine component design [34]. Governing equations used are stated below.

$$\tau_{motor} = \tau_s - \frac{\omega \tau_s}{\omega_n} \qquad (10)$$

$$\omega_{motor} = (\tau_s - \tau)\frac{\omega_n}{\tau_s} \qquad (11)$$

$$P_{motor}(\tau) = -\left(\frac{\omega_n}{\tau_s}\right)\tau^2 + \omega_n \tau \qquad (12)$$

$$P_{motor}(\omega) = -\left(\frac{\tau_s}{\omega_n}\right)\omega^2 + \tau_s \omega \qquad (13)$$

$$V = R * \frac{\tau_i}{k_t} + k_b \omega \qquad (14)$$

$$\tau = V * \frac{k_t}{R} - \omega * \frac{{k_t}^2}{R} \qquad (15)$$

For the design approach, the worst case extremes of the prosthesis joints have been investigated: the peak moment and speed. A single motor and gearing system must be capable of reaching both peaks. Shown in Figure 10, the peak moment and corresponding speed, and vice versa, have been calculated using MATLAB. For simplification of calculations, only these extremes have been tested with the motor initially. It was assumed if a single combination can hit both these extremes, it will be able to do everything in between as well. After a combination was selected, this assumption was verified by checking the calculations along the entire gait cycle.

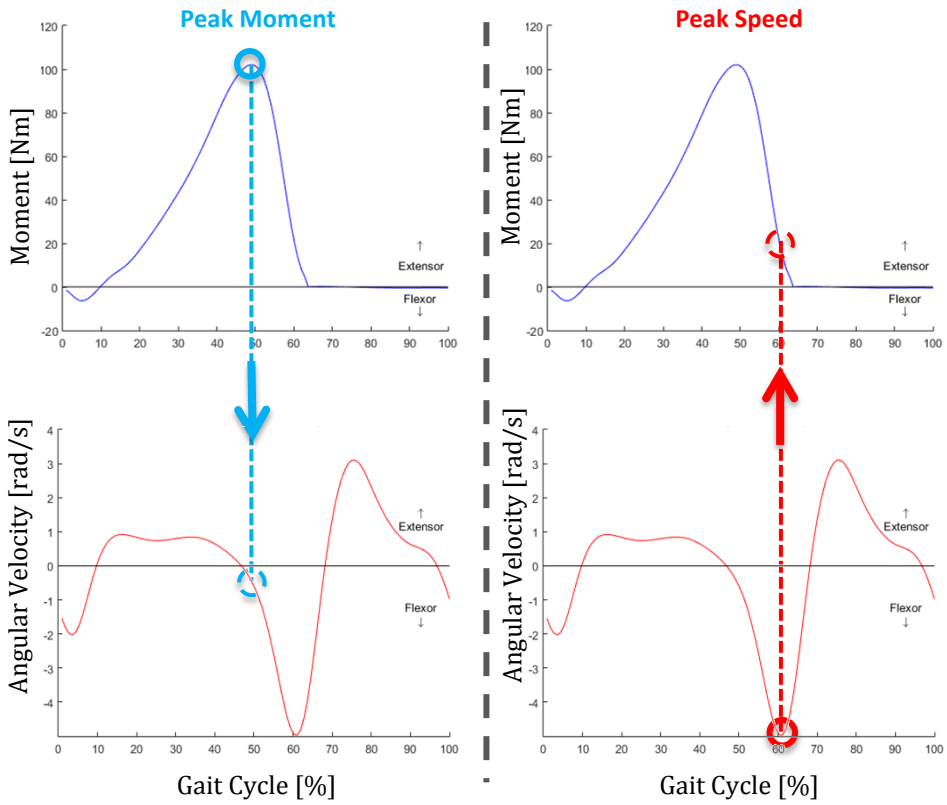

Figure 10. Peak Moment and Speed at Ankle

For the design, the torque, speed (or dependent electric current), and gear ratio have been set as the decision variables. The reasoning is that the actuator must reach a torque to overcome resistance for realizing walking motion and move, so the torque variable has been set to match the joint requirements calculated from the inverse dynamics study in Chapter 2. With joint torque considered fixed, changing the current supplied will change the power and thus change the speed. The required voltage, power, etc., can then be calculated.

3.2.2. OPTIMIZATION

An optimizer has been formulated through MATLAB and EXCEL using macros and has been used to minimize the gear ratio for each motor option while checking if the combination of motor selected and design variables is capable of producing the required loads. The combination with the smallest required gearing and lightest motor is considered the best design. In this design decision, a lower gear ratio is assumed to lead to lighter weigh components which is a design goal. Motor operating calculations in the optimizer are computed based on standard methods from machine component design [34] and the equations stated above (Eq. 10, 11, 12, 13, 14, & 15). Figure 11 provides an example of a single motor and gearing combination from the created optimizer. The left plot represents where the motor needs to operate to reach the highest torque of the gait cycle and the right plot represents where it needs to operate to reach the highest speed of the same gait cycle.

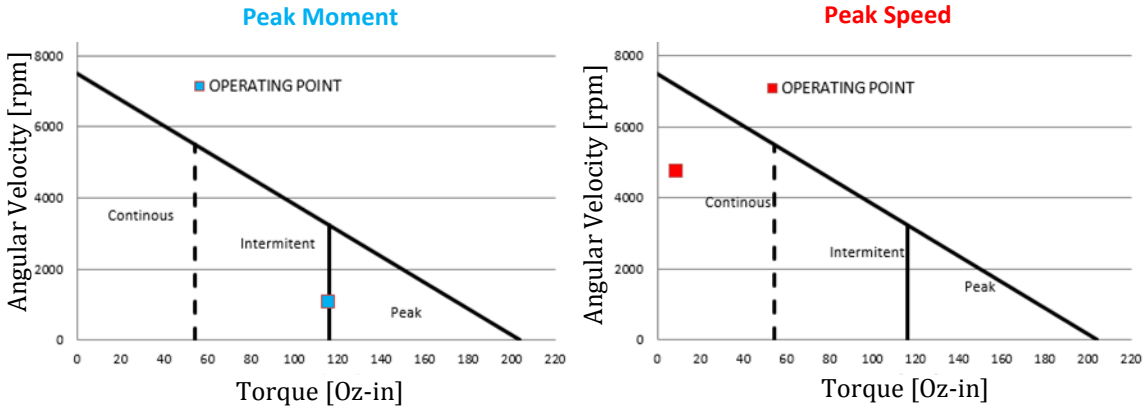

Figure 11. Example Plot of Motor Operating Points

Constraints are checked by comparing the required speed and torque values at the joint and minimizing error (the difference between the required value and operating value) and gearing ratio, with the output from the above example shown below in Figure 12.

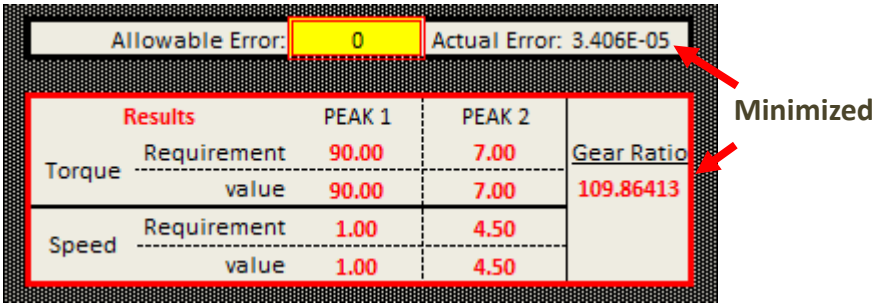

Figure 12. Motor Optimizer Constraint Check

Alternative methods of directly calculating the optimal components or setting up the problem may be possible. For this case with a large database of motor options on hand and many unique situations, taking advantage of optimization tools in the manner described significantly reduced calculations and design time. The following assumptions and simplifications are important to keep in mind for this optimization. The identified components may not be a true optimal design, but is the result of the analysis with these simplifications:

- It has been assumed that, in general, larger gearing ratios will result in heavier components. Gearing ratio is thus minimized as part of the cost function. This is true to in most cases but in reality some off-the-shelf components, such as harmonic drives, advertise varying gearing ratios without any difference in mass.

- The optimizer initially only calculated the worst case extremes when checking if a combination of parameters could meet the requirements.
- Only off-the-shelf options have been considered (Appendix A), and others may still exist that were not included here that are superior.
- The methods of calculating motor performance varied by companies and the meaning of the advertised values used for the calculations vary based on the manufacturer. Here they are treated as the same and the slight difference caused by different methods or parameter identification is neglected.

For the mathematical representation of the optimization problem, the design variables can be written in matrix form as:

$$x = \begin{bmatrix} x_1 \\ x_2 \\ x_3 \end{bmatrix} = \begin{bmatrix} \tau_{motor} \\ GR \\ \omega_{motor} \end{bmatrix} \quad (16)$$

Where:

$$x_1, x_2, x_3 \in \mathbb{R} \quad (17)$$

$$x_2 \geq 0 \quad (18)$$

Two objective functions were considered. The first simply finds a gear ratio (GR) that can meet the requirements while minimizing the ratio. This is to reduce mass and also has other benefits such as improving backdriveability. The second also attempts to

minimize the power required from the motor simultaneously. By testing both functions more of the design space was explored.

Objective Function 1:

$$\min\left(E_{total}(x_1, x_2, x_3) + W_{GR}x_2\right) \qquad (19)$$

s.t. (24), (25), (26), (27)

Objective Function 2:

$$\min\begin{pmatrix} E_{total}(x_1, x_2, x_3) + W_{GR}x_2 \\ +I_{peak1}(x_1, x_3) + I_{peak2}(x_1, x_3) + \tau_{peak1}(x_1, x_3) \end{pmatrix} \qquad (20)$$

s.t. (24), (25), (26), (27)

Objective function 2 was found to be more capable of finding motor operating points that could use smaller gear ratios and ultimately found better solutions (lower gearing ratios) than objective function 1. Error (E_{total}) was calculated with equations 21-23, comparing how far the resulting value is to the requirement. E_τ is the error from torque and E_ω is the error from speed. W_{GR}, W_τ , and W_ω, are penalty scaling constants for the gear ratio, torque, and speed, respectively. These scaling "weight" values, defaulted to 1.0, are used to change how much each value impacts the optimization, such as a penalty scaling constant. I_{peak1} and I_{peak2} are the motor currents at the torque and speed extremes for the motor. τ_{joint} and ω_{joint} are the resulting torque and speed at the

joint after the gear ratio is applied. $\tau_{requirement}$ and $\omega_{requirement}$ are the required values for torque and speed at the joint, obtained from the biomechanics analysis.

$$E_{\tau}(x_1, x_2) = \left|1 - \frac{\tau_{joint}(x_1, x_2)}{\tau_{requirement}}\right| W_{\tau} \quad (21)$$

$$E_{\omega}(x_2, x_3) = \left|1 - \frac{\omega_{joint}(x_2, x_3)}{\omega_{requirement}}\right| W_{\omega} \quad (22)$$

$$E_{total}(x_1, x_2, x_3) = E_{\tau}(x_1, x_2) + E_{\omega}(x_2, x_3) \quad (23)$$

Several constraints and design bounds have been applied to the optimization:

$$E_{total}(x_1, x_2, x_3) \leq E_{allowable} \quad (24)$$

$$0 < \tau_{motor}(x_1) < \tau_{\max\_limit} \quad (25)$$

$$0 < \omega_{motor}(x_3) < \omega_{\max\_limit}(\tau) \quad (26)$$

$$0 \leq I(x_1, x_3) \quad (27)$$

Error (E_{total}) was given an allowable limit ($E_{allowable}$) for the purpose of relaxing constraints and exploring more of the design space while using the optimizer. Generally, a value of zero was used and is desired. Small values have been introduced when the optimizer could not find a solution. In cases where no solution could be found, weighted values (W_{GR}, W_{τ}, W_{ω}) have been modified to force the optimizer to place importance on

satisfying specific constraints over others, such as meeting the torque requirement and relaxing the speed requirement, when meeting both was not possible.

The torque and speed maximum limitations listed in the constraints vary based on the motor specifications. These motor limits are defined as τ_{max_limit} and $\omega_{max\_limit}(\tau)$. The requirements tested in equations 21 and 22, $\tau_{requirement}$ and $\omega_{requirement}$, are from the biomechanics analysis and are limits from human data. The governing equations are stated in Equations 10-15.

The most challenging torque and power requirement for the prosthetic is from the ankle joint which must meet high values to properly mimic a healthy human gait. Motors must be chosen which can generate torques high enough to meet this requirement and can often be heavy and result in higher energy expenditure of the user. The created optimizer was unable to find a realistic combination of motor and gearing to meet the theoretical worst case values in the ankle for multi-contact walking. By application of elastic elements as discussed in the introduction, however, the power requirements of the motor can be significantly lowered. To complete the motor and gearing selection, constraints for the motor and gearing selection have been relaxed to the values from the experimental walking data rather than the theoretical worst case so the optimizer could find a solution.

Harmonic drives provide large gearing ratios in small profiles and are frequently used on prosthetics, including with AMPRO II. The harmonic drives are, however, by far the heaviest components of the assembly. As such, they were initially avoided in the design in favor of light gearboxes. An off-the-shelf gearbox rated with properties high

enough to handle the torques of the prosthetic has been tested in an early iteration of the prosthetic design, shown in Figure 13. A custom testing rig was created to verify each gearbox could safely handle the torques. The testing results, however, showed one box failed by stripping the threads off one of the gears. Confidence in this method being safe was not high and the design was dropped. Moving forward harmonic drives have been chosen for the gearing to ensure safety and longevity of the device. The failed method is still worth mentioning here, however. As the harmonic drives are the heaviest components in the assembly, finding an alternative gearing method with less mass in the future will be highly beneficial (the gearboxes tested here were lighter by roughly a factor of 10). It is likely a custom designed gearbox will be capable of the requirements. For this design however, due to funding and timing restrictions only off-the-shelf components are used and as such the more reliable harmonic drives have been selected.

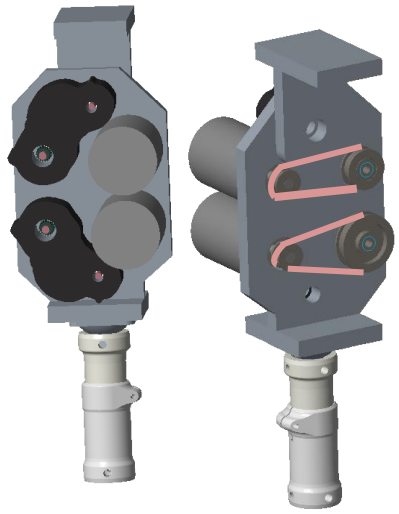

Figure 13. Failed Gearbox Design Concept

3.2.3. Optimization Results

The methods described for the motors and gearing were not able to find any combinations that could reach the theoretical worst case values from Figure 8. Moog Motor Company was also contacted to verify; the engineers confirmed they could not meet these requirements. An example of such an attempt is shown below using motor BN28-29AF-01.

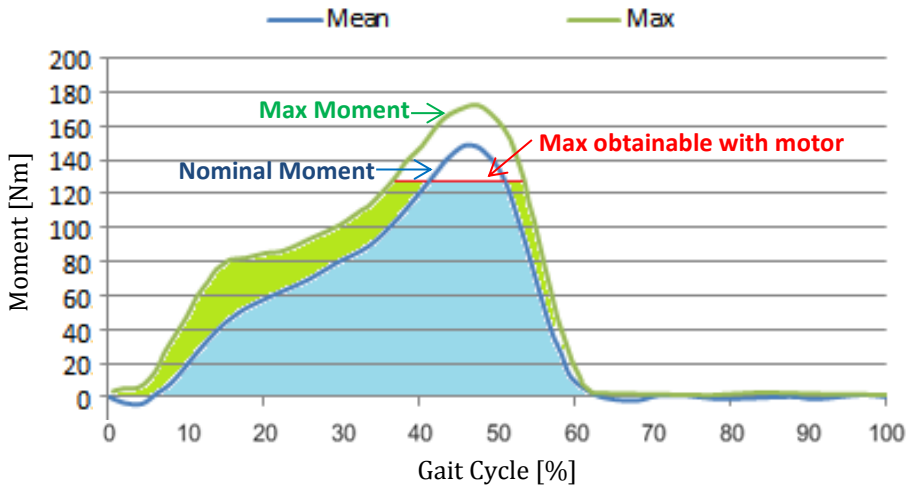

Allowable Error:	0	Actual Error: 0.2858152	
Results		PEAK 1	PEAK 2	
Torque	Requirement	172.00	46.00	Gear Ratio
	value	133.77	46.00	189.41959
Speed	Requirement	0.80	4.50	
	value	0.80	4.50	

Figure 14. Optimizer Attempt to Reach Worst Case Values

Shown above, if considering the worst case we can design towards one peak or another, but not all 4 requirements. The combination above was able to meet the requirements for speed for both peaks but only torque for one. This brings us to a

conclusion that the inclusion of a spring force or other stored energy method must be used to mimic the joint dynamics for the worst case values.

As discussed, to select the motor and gearing the constraints were relaxed and requirements lowered to the values calculated from the human walking data. The captured human walking data gave a more realistic ankle torque value of 100Nm (as opposed to 172Nm), shown below. The optimizer was able to meet this curve using a Maxon 429271 motor paired with a gearing reduction of 90.

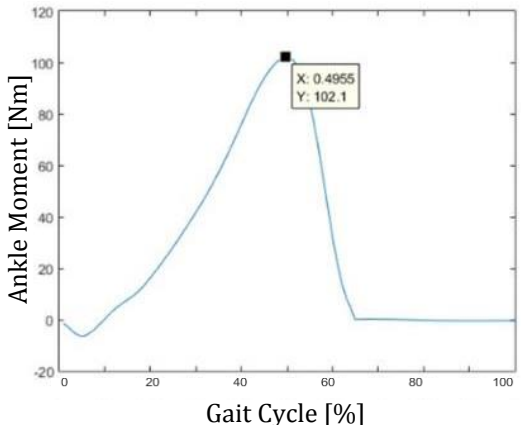

Figure 15. Captured Ankle Torque from Human Data

Moving forward, a Maxon 429271 motor has been paired with a harmonic drive with a ratio of 120 for the ankle. The proposed design (Figure 62) has one additional gearing stage for the ankle after exiting the harmonic drive due to the belt connecting to the joint. This allows a high range of ratio adjustments using the pulleys as another gearing stage. It is noted that the 100Nm torque from the human data is on the low end of published ankle torque values so by using a ratio of 120 at the harmonic drive the torque capabilities of the prosthetic will stay in the middle of the range. Sizing the

pulleys larger or smaller after the H.D. will bring the ratio up or down as needed if a person has vastly different torque/speed needs and in this case it can be used to bring the ratio back down to 90 for this user, as was suggested by the optimizer. It is impossible to select a motor and gearing that will be perfect for everyone, but this selection was chosen to try to capture acceptable performance for as many people as possible.

3.3. Elastic Elements and Walking Simulations

In this thesis, several elastic energy saving components have been investigated. Walking simulations have been manually coded in MATLAB for these investigations. Initially the methods described for inverse dynamics have been applied using a walking simulation of human data plotted from the experiment mentioned in Chapter 2. Springs and other components are then added to the calculations and simulation. In a case using a spring, the compression of the spring from the natural walking pattern is calculated with the resultant spring force. This force is then added to the calculations of the link-segment-model and required motor power estimated. Calculations using this method have been computed on a LSEA to assist in validating the design method. The LSEA simulation analysis returned nearly identical results to the benefits published in literature [9]. It should be noted however that this analysis is based on inserting the spring force into the inverse dynamics with the same force and kinematic data, with the assumption that if those data points stay constant the resulting requirements of the spring and motor can be estimated. This is a necessary assumption for the analysis but should be backed up with physical testing.

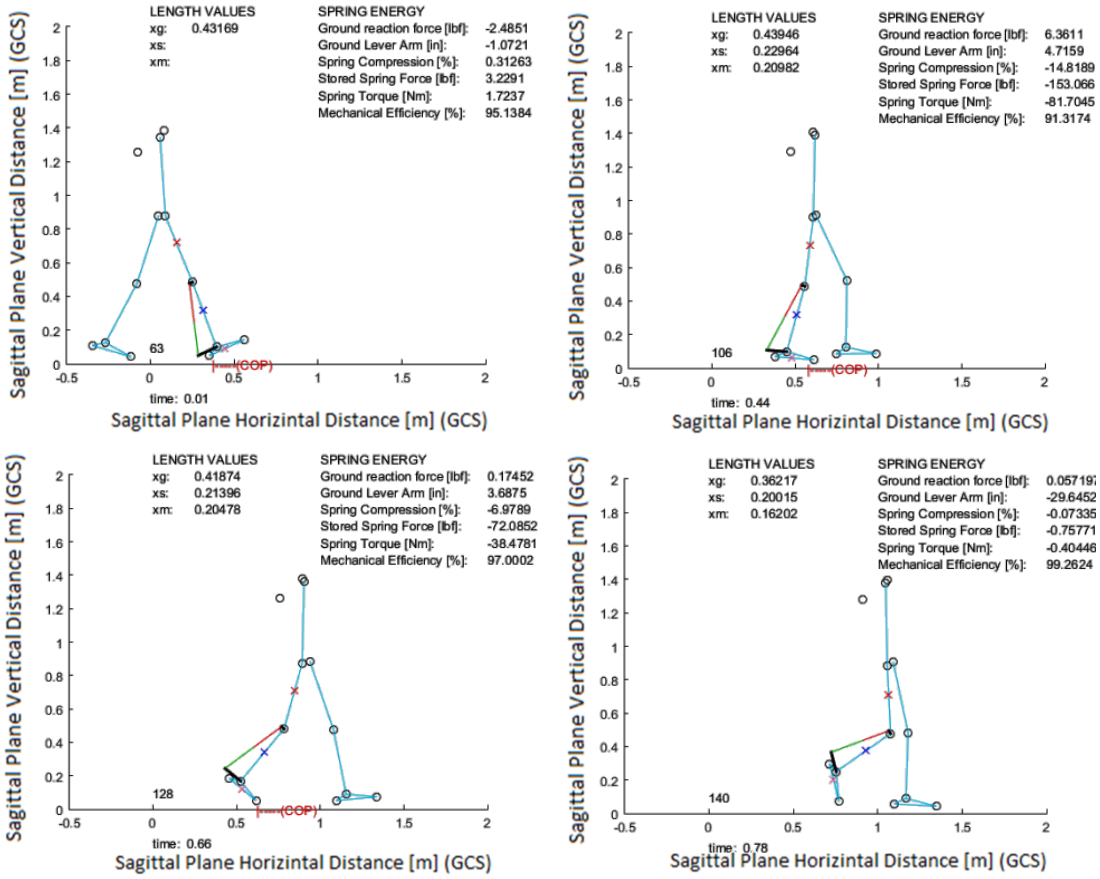

Figure 16. Example Walking Simulation of Elastic Elements

Shown above in Figure 16, a linear series elastic actuator has been used in one walking simulation. As the center of pressure (COP) moves across the foot, the distance to the joint and force values are used to calculate the forces and moments in the joints. The black bars represent mounting moment arms, the green line is the spring, and the red line is the linear actuator. Using basic trigonometry the compression of the LSEA has been calculated. Calculating the length of the spring and linear actuator with resulting power follow methods from Hollander et al. [9].

Seen from Figure 16, the angle of the LSEA changes and it is not always perpendicular to the moment arm. This has been neglected in published literature but taking this angle into account shows the moment applied at the ankle will be lowered as only the perpendicular component of the vector helps with the torque and the horizontal component will go into the frame. Changing the length of the black moment arms in Figure 16 changes this angle. For a specific length, the percentage of the force that is perpendicular is plotted below in Figure 17 and shown with the power. For an improved design, the length of the moment arms can be adjusted to line up the high angle efficiency values with the high power values.

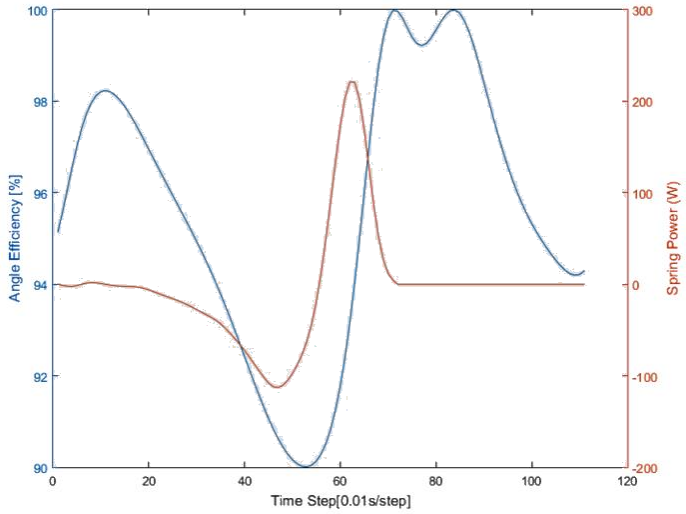

Figure 17. LSEA Angle Impact

The length of the moment arms described above has been varied in a simulation along with the stiffness of the spring. The resulting required power from the motor based on variations of the spring stiffness is shown in the following figure.

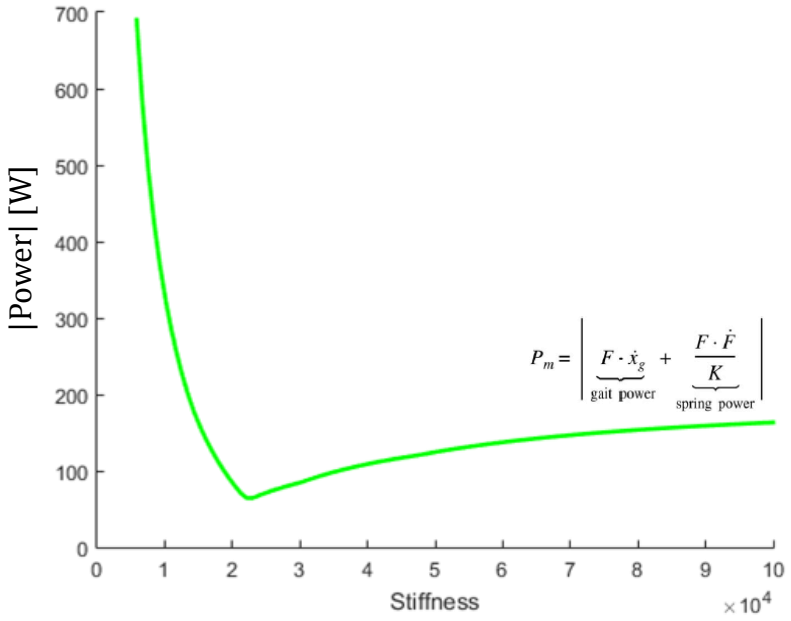

Figure 18. Power Required from Motor Based on Spring Stiffness for LSEA

The plot of power based on stiffness matches expectations based on published values from Hollander [9] and serves as a validation of this design approach. The optimum stiffness is the value in the corner that gives the lowest power number (this is the power required from the motor to walk).

The simulation has been run in iterations to find the optimum design based on varied moment arm lengths and stiffness values. The resulting power values are shown in the following figure. These values also closely match published values.

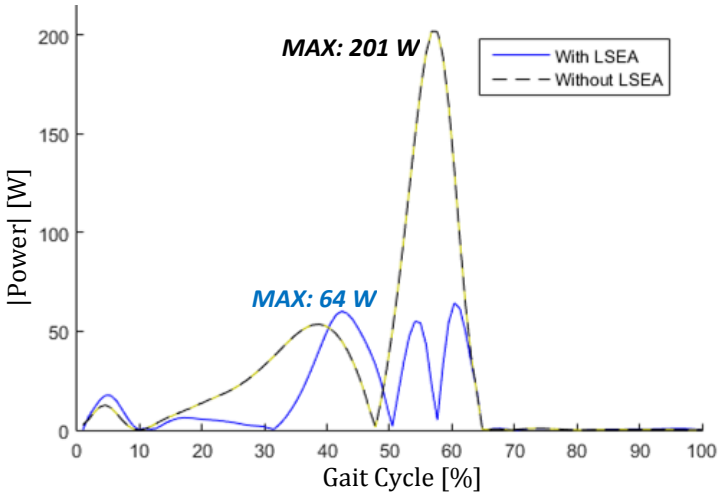

Figure 19. Power Values from LSEA Simulation

In this thesis, other elastic energy saving components have also been investigated. Each is designed based on similar MATLAB simulations to that described for the LSEA. Other concepts tested using this method include a pre-loaded spring at the ankle (described in Chapter 3.4), springs in the toe joint, and a RSEA.

An example from the toe joint spring simulation is shown in the following figure. In this case a new joint was modeled in the foot to incorporate the toe, which is usually neglected. The bending and angles of the toe have been calculated. The pink portion represents a spring secured to each side of the toe joint. As the toe flexes, the spring compresses. The resulting forces and moments have been investigated through inverse dynamics to see if this will improve the efficiency of the prosthetic. In the simulation shown, the dotted lines represent the angle the force vectors from the compressed spring will act. For this analysis one method of estimating impact is to add these forces to the moment calculation around the ankle joint, with distance calculated from the dotted lines. An alternative method is to fully separate the toe joint and only incorporate the

forces for that toe segment separately, following by a reaction calculation along the back of the foot, which is the typical link-segment model method. Results of the simulation show this could be beneficial. Optimization work should adjust the connection points of the toe-spring to control the vector path of the spring forces.

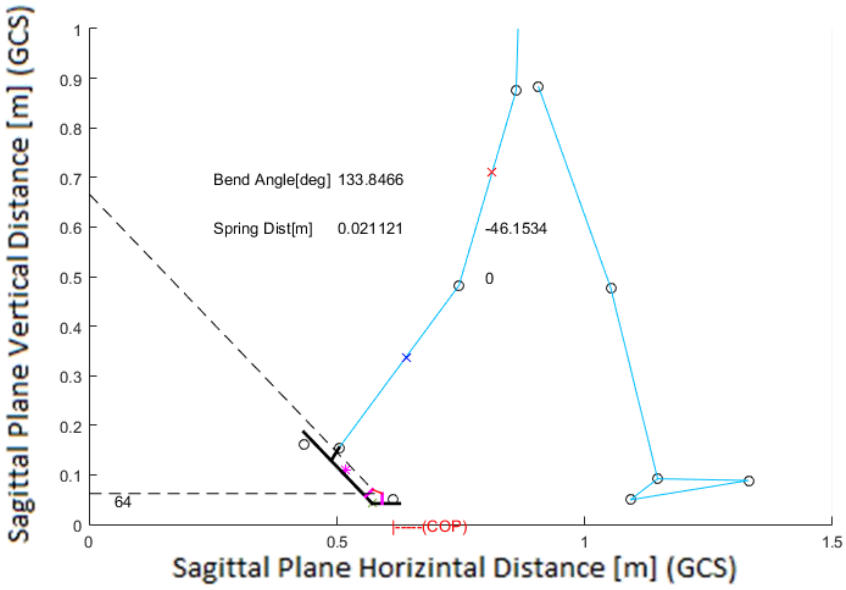

Figure 20. Toe Springs Simulation

The accuracy of the methods used to calculate the impact of the toe joint springs cannot be validated without physical testing. For the design in this thesis, such a design is not being used. For future work, however, this shows potential and should be further investigated. This decision was based on keeping the scope of the research realistic and does not necessarily imply the chosen concepts will be superior to the toe springs. Such a design as represented by Figure 20 requires a completely custom designed foot which is not part of the project.

3.4. ANKLE SPRINGS

One of the optional "add-on' components that has been investigated in this thesis is a pre-loaded spring on the ankle. This concept looks similar to a LSEA but consists only of a pre-loaded spring on the ankle without the actuator. The concept is shown below in Figure 21. In this simulation the black bars are moment arms and mounts while the green line is the spring. As the joints bend in the simulation, the resulting length of the spring has been calculated as well as the spring force impact on the rest of the system.

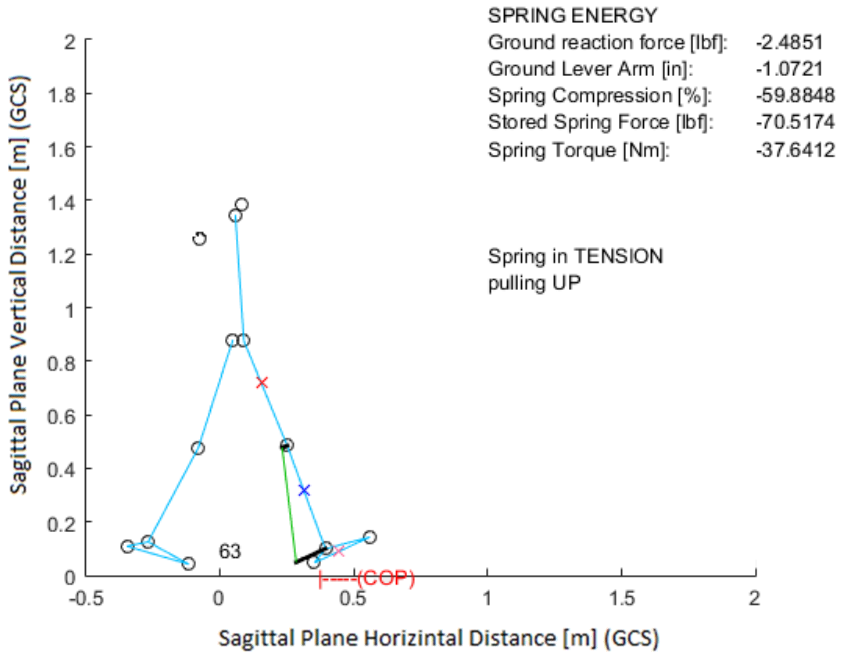

Figure 21. Preloaded Ankle Spring Simulation

With this addition preloaded spring torque on the ankle, the motor must only make up the difference between the pre-loaded value and the required joint value. When

the spring is applied, the torque profile generated by the motor is almost identical to not having the spring but it is effectively shifted up, as shown in Figure 22.

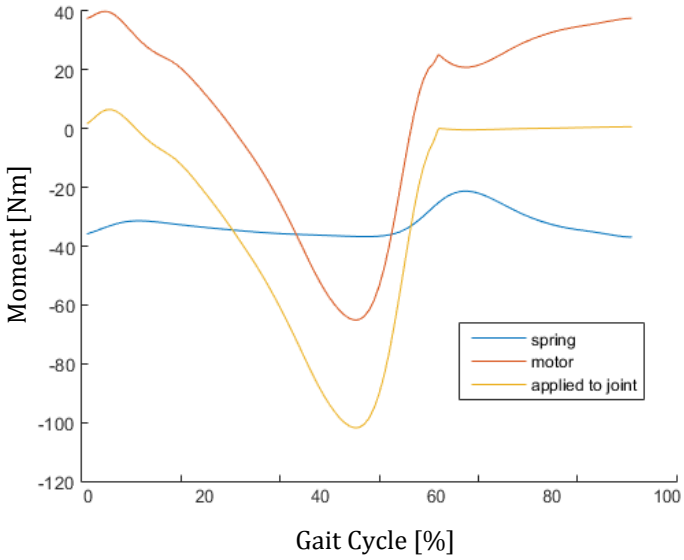

Figure 22. Ankle Spring Moment Calculations

The power required of such a system shows potential benefits; maintaining the shifted torque curve requires a motor capable of significantly lower power magnitudes. Shown in Figure 23, throughout the gait cycle the maximum power magnitude required by the motor has been theoretically reduced in half. This reduction has been accomplished through optimization of components in the system through simulations. A screenshot from such a simulation is shown in Figure 21 and follows the methodology described above for similar simulations. The stiffness and length of components (moment arms, spring size, etc.) in that simulation have been left as variables as the resulting motor power was minimized. The downside is clear by viewing the power

curve, Figure 23. Towards the end of the gait, zero torque is desired at the ankle and the motor must now counteract the pre-loaded spring. This results in extra power now required at the end of the gait as shown in Figure 23. This extra power is however only over a small percentage of the gait. Rather than having a high-torque motor to reach the high magnitudes of the ankle, a low-torque motor can be run in its place; it just needs to run for a longer period of time. Magnitude differences are shown in Figure 23, roughly 200W compared to 100W. A lower torque requirement on the motor means much smaller and thus lighter motors can be used to reduce energy expenditure of the user. Patrick et al. [4] through analysis of the current generation of powered transfemoral prosthetics at Texas A&M, AMPRO II, has identified the mass of the prosthetic to be a primary cause of increased energy expenditure of the user so this tradeoff is worth further investigation. From the simulated concepts, this design has been chosen to move forward for future physical prototypes. Physical design concepts have been generated for this as an optional component in CAD and the intended design is described in the following section.

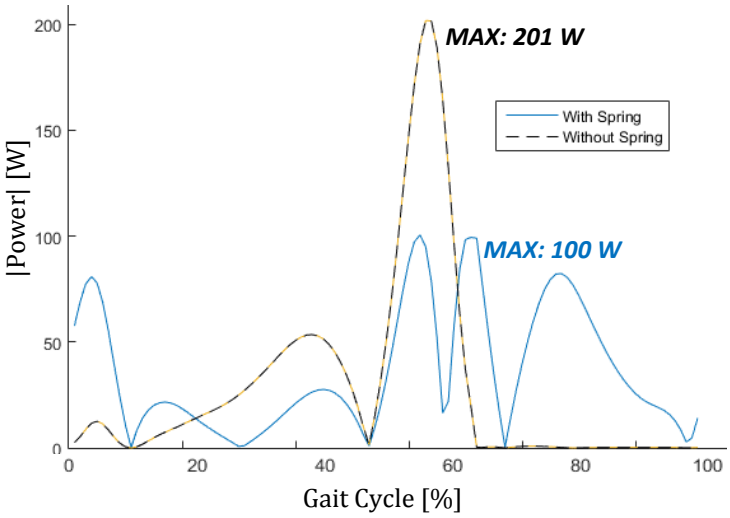

Figure 23. MATLAB Walking Simulation

3.4.1. Ankle Spring Physical Design

With the optimal stiffness of the ankle springs found through simulation, components need to be created and mounted in a way that that is modular to keep in line with the design goals. The ankle joint has been designed such that plates can extend out from above and below the rotation and act as moment arms. At the end of these moment arms several off-the-shelf springs can be secured to add up to the required stiffness value. A CAD model of the design is shown in Figure 24.

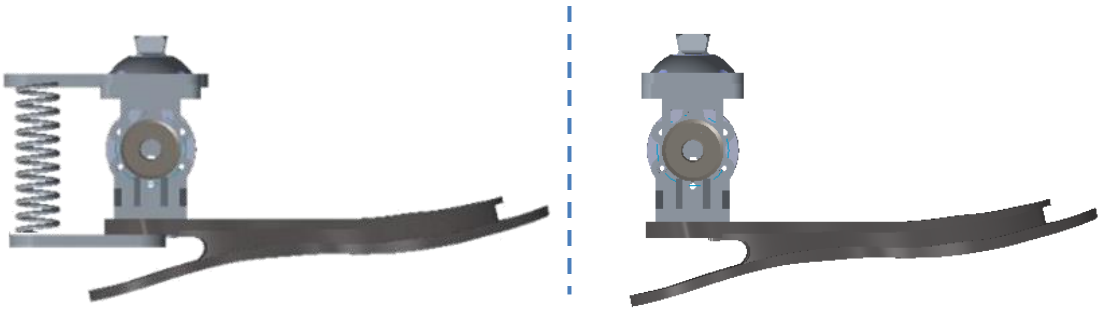

Figure 24. Modular Ankle Spring Components

The design shown in Figure 24 represents the ankle springs installed (left) and removed (right). The top spring mounting bracket is sandwiched between the pyramid adapter and the upper ankle bracket. The bottom spring mounting bracket is secured to the bottom of the foot as shown. Existing mounting holes and hardware will be used.

3.5. Rotary Series Elastic Actuator

In an effort to gain the benefits of the linear series elastic actuator (LSEA) with less mass and complexity, the methodology employed by Hollander et al., [9] has been applied to a rotary series elastic actuator (RSEA). As mentioned, a downside of the linear series elastic actuator is the requirement of additional mechanisms and lever arms on the back of the leg. Initial design concepts and methods for the RSEA follow those being used for improvement to control and safety [17]. The work of Hollander et al. [9] has then been used to estimate the required motor power with the presence of such a spring. Though, in this case the math has been applied to a rotary spring rather than linear. The calculation of power is thus calculated as follows, with reference to Figure 25:

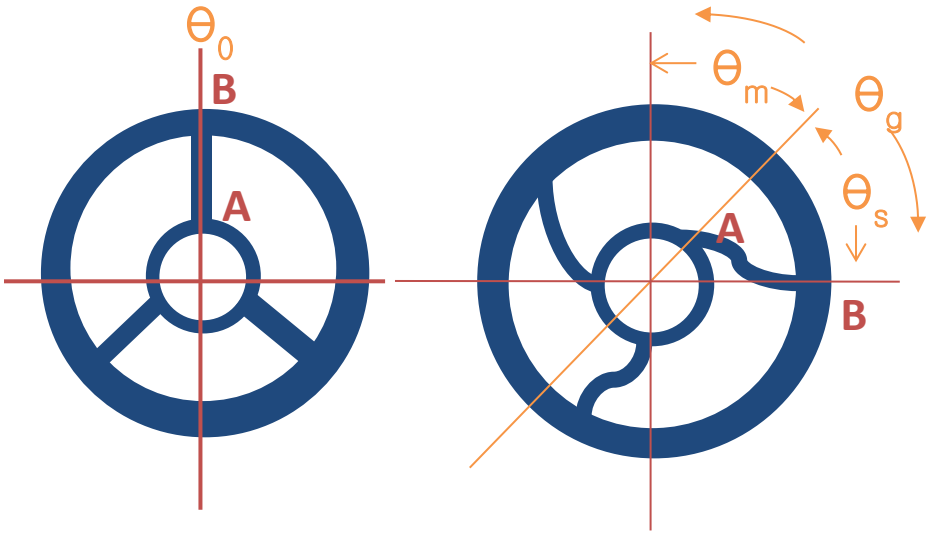

Figure 25. RSEA Deflection

From the diagram above, the angles are:

$$\theta_g = \theta_m + \theta_s \quad (28)$$
$$\rightarrow \theta_m = \theta_g + \theta_s \quad (29)$$

$$\Delta\theta_s = \theta_s - \theta_0 \quad (30)$$
$$\rightarrow \theta_s = \Delta\theta_s + \theta_0 \quad (31)$$

The moment from the spring can also be included to generate the following:

$$M = K\Delta\theta_s \quad (32)$$
$$\rightarrow \Delta\,\theta_s = M/K \quad (33)$$

Combining Equation 31 and Equation 33:

$$\theta_s = \frac{M}{K} + \theta_0 \quad (34)$$

Combining Equation 29 and Equation 34:

$$\theta_m = \theta_g - \frac{M}{K} - \theta_s \quad (35)$$

Taking the derivative:

$$\dot{\theta_m} = \dot{\theta_g} - \frac{\dot{M}}{K} \quad (36)$$

Calculating the power of the spring, motor, and total (gait):

$$P_s = M\dot{\theta}_s = M\left(\frac{\dot{M}}{K}\right) \quad (37)$$

$$P_g = M\dot{\theta}_g \quad (38)$$

$$P_g = P_s + P_m \quad (39)$$

Solving for the required motor power:

$$P_m = P_g - P_s = M\dot{\theta}_g - M\left(\frac{\dot{M}}{K}\right) \quad (40)$$

Simplifying:

$$P_m = M\left(\dot{\theta}_g - \frac{\dot{M}}{K}\right) \quad (41)$$

Here P_m is the power required from the motor, $\dot{\theta_g}$ is the velocity of the total spring deflection, $\dot{M}$ is the first derivative of the moment, and K is the spring stiffness. Parameters have been optimized through simulations in MATLAB to come to the ideal spring constant based on the moments required at the ankle joint. This method is nearly identical to that published by Hollander et al. [9] but applied to a rotational spring instead of a linear. Equation 41 is minimized as an optimization in a MATLAB simulation. Results of the optimization are described in the following section.

3.5.1. RSEA RESULTS

Results from the RSEA design show similar improvements to the linear SEA concept. Shown below in Figure 26, by taking advantage of the energy in the spring the theoretical power requirements of the motor are lowered from 201 W to 52 W (the LSEA in literature was estimated to lower requirements from 250 W to 77 W).

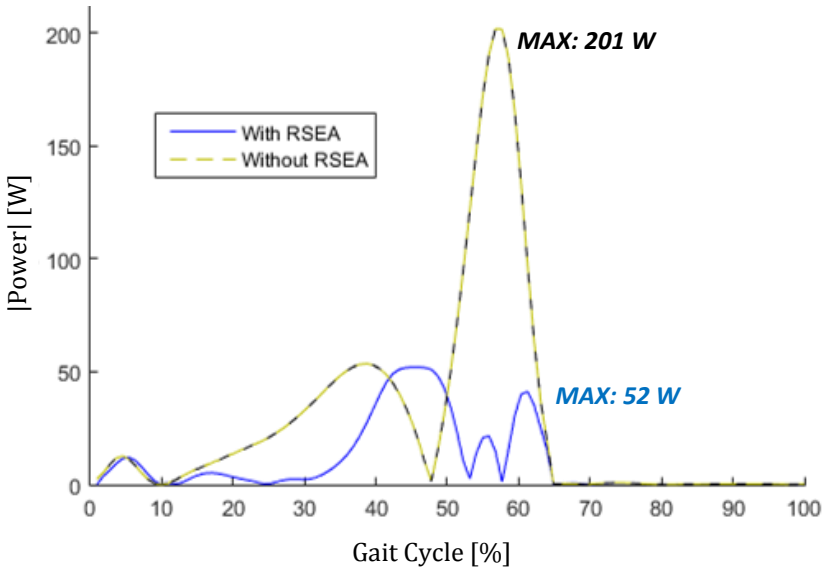

Figure 26. Torsional RSEA Optimized for Power

Designing a torsional spring capable of the simulated result shown in Figure 26 requires deflection of up to 20 degrees without yielding the material of the spring. Upon investigating existing RSEA designs, however, they tend to have a maximum deflection of around 5 degrees [15, 17]. To improve the feasibility of the research and keep in line with successful publications, deflection is being limited to smaller numbers such as 5 degrees for initial investigations. With this constraint, the estimated benefit is now reducing a calculated 201W to 140W.

3.5.2. RSEA Physical Spring Design

The RSEA spring is a disk that must mount the outer edge to a pulley and the inner edge to the harmonic drive. Rotary deflection must take place between the inner and outer edge of the disk without any major radial deflection. To design the disk, the mounting points on the outer and inner section of the disk have initially been modeled with no connection. Material has then been added to connect the inner and outer disk. For initial concepts, the shape of the material connecting the inner to outer portion of the disk has been based on designs found in literature [17]. Examples of design concepts from Phalen, et al. are shown in Figure 1.

Similar shapes to literature for connecting the inner and outer disks have been modeled in CAD. In each case, the shape has been defined systematically with specifically sized connecting arches or loops rather than random splines. By defining it as a combination of arches or loops, the size can be systematically iterated more easily by changing the thickness, angles, etc., of the connected arches based on analysis results. This is shown in Figure 27 with the adjustable arc structure shown on the left and the final disk design from this iteration on the right. A second design shape is shown in Figure 28.

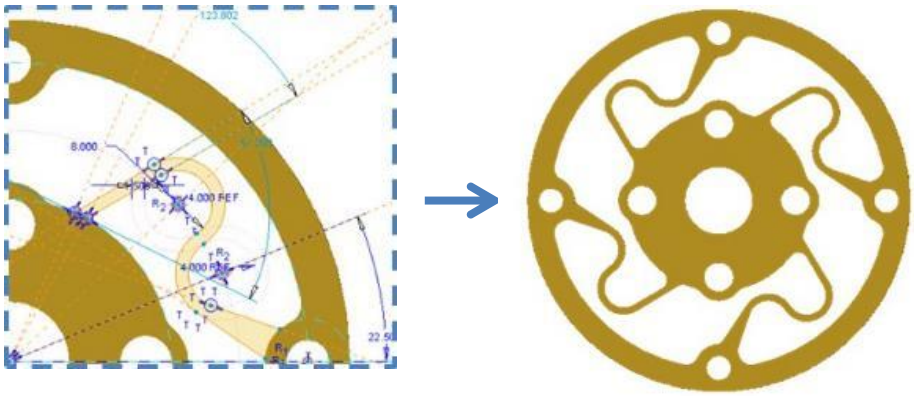

Figure 27. RSEA Design Generation Shape 1

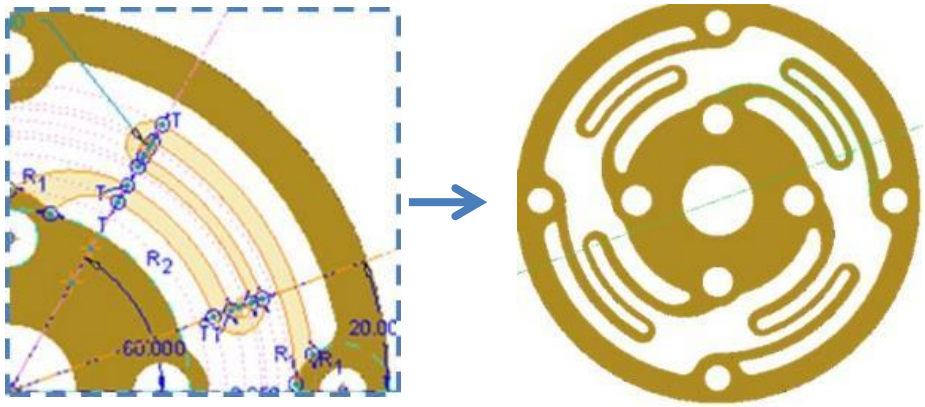

Figure 28. RSEA Design Generation Shape 2

The maximum torque value at the ankle is known from biomechanics data and the experiments run. The deflection angle for the optimum spring design is also known from the MATLAB simulation. To design the spring, it becomes a simple static analysis. With a known torque, it needs to have a known deflection. The size of the connecting arches and loops have thus been modified and iterated through FEA analysis runs until those two numbers are met. More details of the analysis can be found in the structural design section.

3.5.3. RSEA Assembly Design

Space restrictions made connecting the RSEA torsional spring to the pulley difficult (see the results section for how the assembly connects). The outer disk needed to expand far enough out to provide room for the deflecting elements between the inner and outer disks. At the same time, making the disk radius too large interferes with parts and makes mounting the pulley more difficult. To get around the mounting issue the assembly has been designed as three separate parts. The spring segment has been designed as a flat disk to reduce manufacturing costs. The connecting part is aluminum with threads and a mount for the pulley. The pulley is then secured to the aluminum mounting disk. The end result, shown in Figure 29, is that the pulley will have an elastic element of deflection between itself and the harmonic drive.

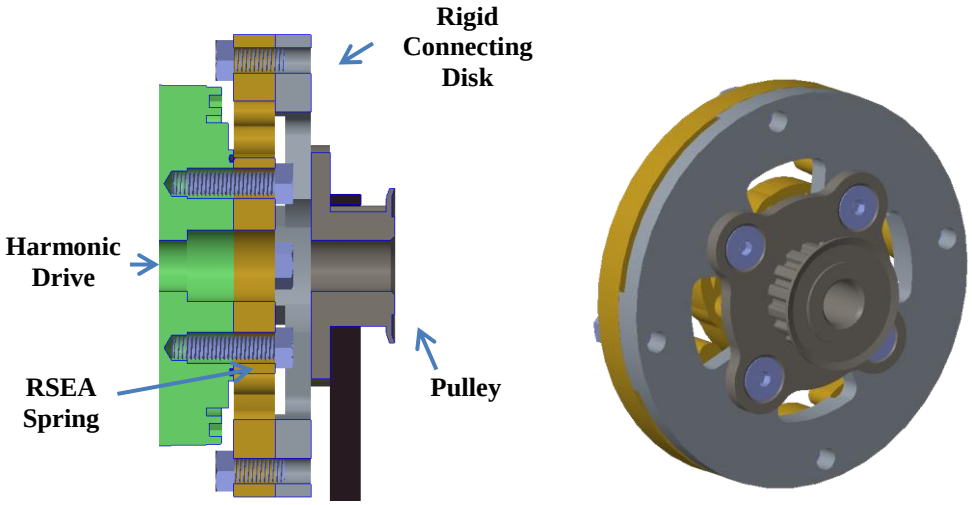

Figure 29. RSEA Assembly

3.6. Ankle Joint Modular Options

3.6.1. Rigid Ankle Joint Option

As elastic elements are intended to be modular, a mount has been designed to directly connect the harmonic drive to the pulley without any elastic elements (removing the RSEA torsional spring). The design is shown in Figure 30. It was created by simply aligning hardware holes.

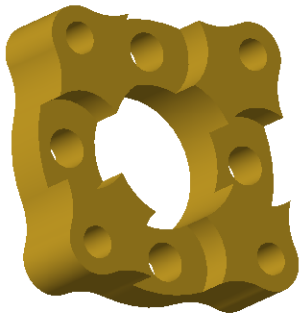

Figure 30. Rigid Ankle Joint Mount

3.6.2. Changing Components

Mounting options of the RSEA spring and rigid mount are shown in Figure 31. Both can easily be installed as shown. For experimentation, the spring design can also be changed to one with more or less stiffness depending on the needs of the user or researcher.

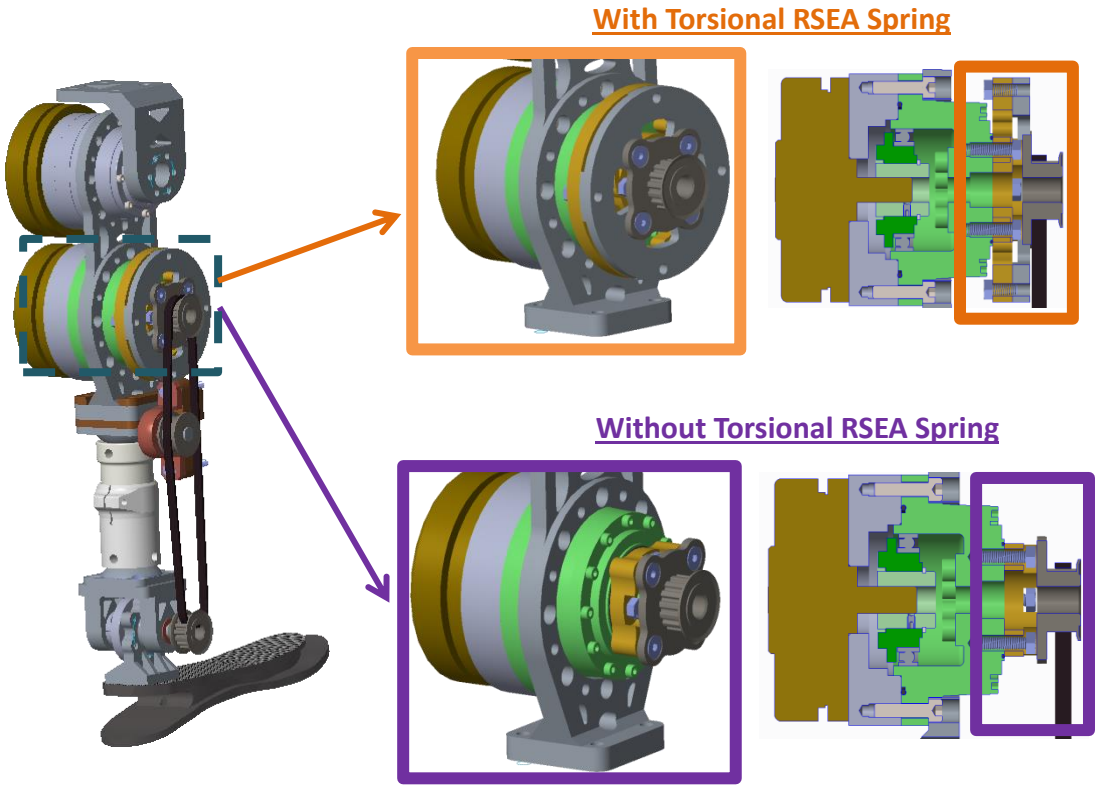

Figure 31. Ankle Joint Elastic Options

3.7. Height & Leg Adjustment

To take into account use for different users, one of the design goals is easy adjustability. AMPRO II currently cannot be adjusted at all, due to the design consisting of a single frame as shown in Figure 3. From literature reviews, pylons have been identified as a standard method of adjusting height, such as was incorporated by Vanderbilt University shown in Figure 2. Such a pylon helps but is still a set length; adjustments require a new part cut and manufactured which is not ideal. A new adjustable pylon from Kinetic Revolutions has been identified and is used in this thesis

to mitigate the problem. Shown in Figure 32 the pylon is two parts with an internal screw allowing adjustment on the fly.

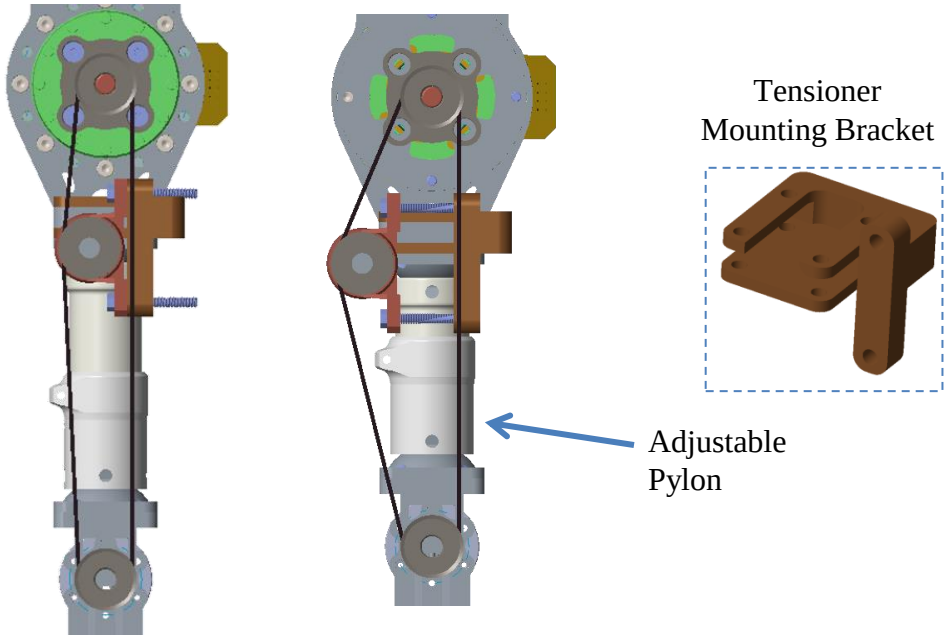

Figure 32. Adjustable Pylon & Belt Tensioner

As a belt must connect across the adjustable area, a belt tensioner was developed for this case. It connects with a 3D printed bracket shown on the right in Figure 32. The custom bracket wraps around the bottom of the frame to reduce required mounting space. As the tensioner will not see any significant loading, 3D printing was chosen to manufacture this custom shape. A high strength printed material will still be used for safety (various metal alloys are being investigated). As a backup, a machined metal bracket can also be used in place of the 3D printed version.

The center image in Figure 32 shows how the tensioner works. An off the shelf pillow block and custom pulley move further away from the frame bracket with screws.

Using screws allows fine tuning to get exactly the distance required. If the pillow block must be pushed out significantly more and it becomes aesthetically an issue, a filler part can be placed in the middle. For use on alternate legs, the motors must always be facing the medial side of the user. The foot can be rotated to face in the correct direction for this case.

4. GEOMETRY AND STRUCTURAL DESIGN

4.1. MODEL SETUP

Structural components have been minimized to further reduce weight. Components have been designed by loading each part in an FEA analysis. Material is added so each part is capable of withstanding walking loads with unnecessary material removed to reduce weight.

4.1.1. SIMPLIFICATIONS

To reduce computational costs of the analysis, several simplifications have been made. Rather than loading the entire assembly at once, the upper and lower portions of the assembly have been analyzed separately. CAD geometry of some parts have also been simplified as meshing the complex components significantly increases computational costs. None of the important structural components being designed have been simplified in such a manner. An example of the simplification is shown in Figure 33.

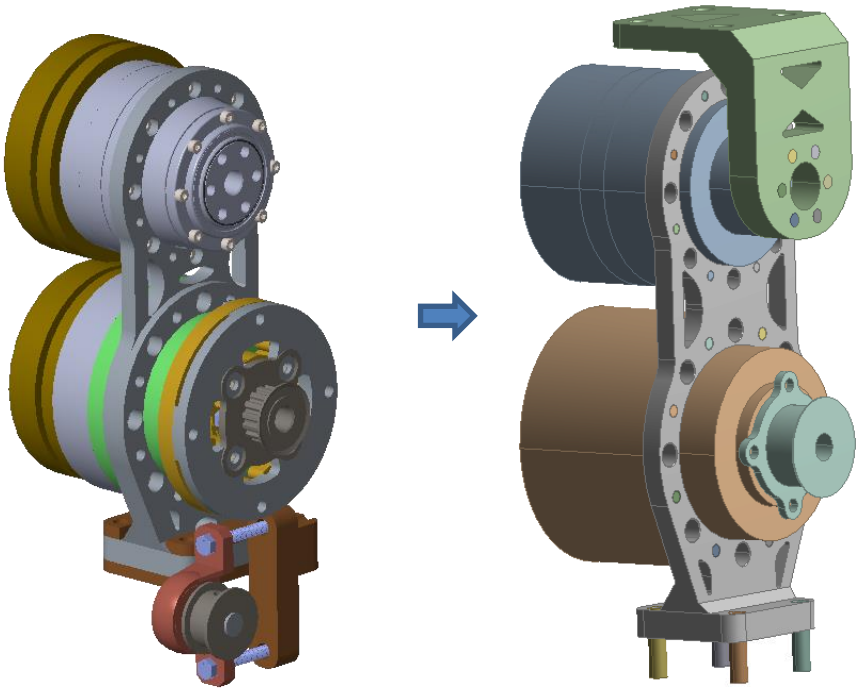

Figure 33. FEA Geometry Simplification

4.1.2. Interface Conditions

Connections have been simplified by modeling the bolts as cylinders and joining the meshes of touching parts through “perfectly bonded” connections. This is shown in Figure 34.

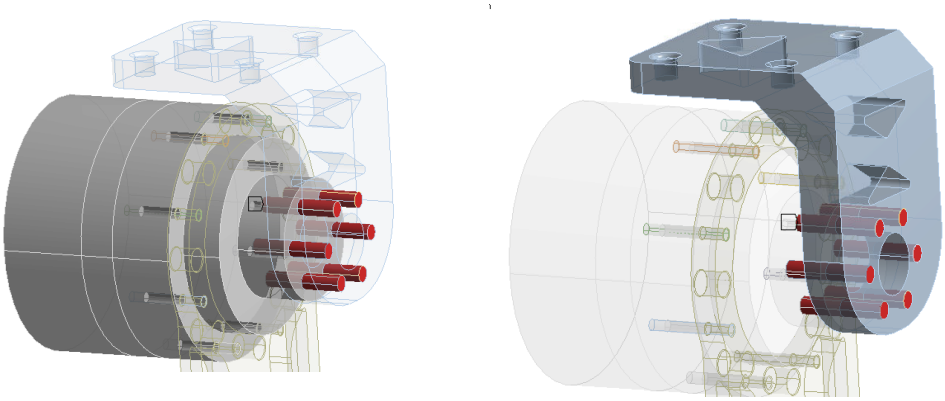

Figure 34. FEA Connections/Interface Conditions

The interfaces shown in Figure 34 are similar to those used for other parts as well. For a complete list of conditions used, see Appendix B.

4.1.3. FEA Design Method

From the stated load cases below, designs have been iterated in an attempt to minimize material. Locations of high stress have been reinforced and material has been removed from locations of low stress, such as by adding holes. An example of such an iteration is shown in Figure 35, which is plotting safety factor. As seen in the image, holes have been removed around the orange section to strengthen the part and the upper section was increased in thickness. Also clear from this iteration, there is a lot of unnecessary material on the top of the frame. A hole was added to accommodate this with the next iteration.

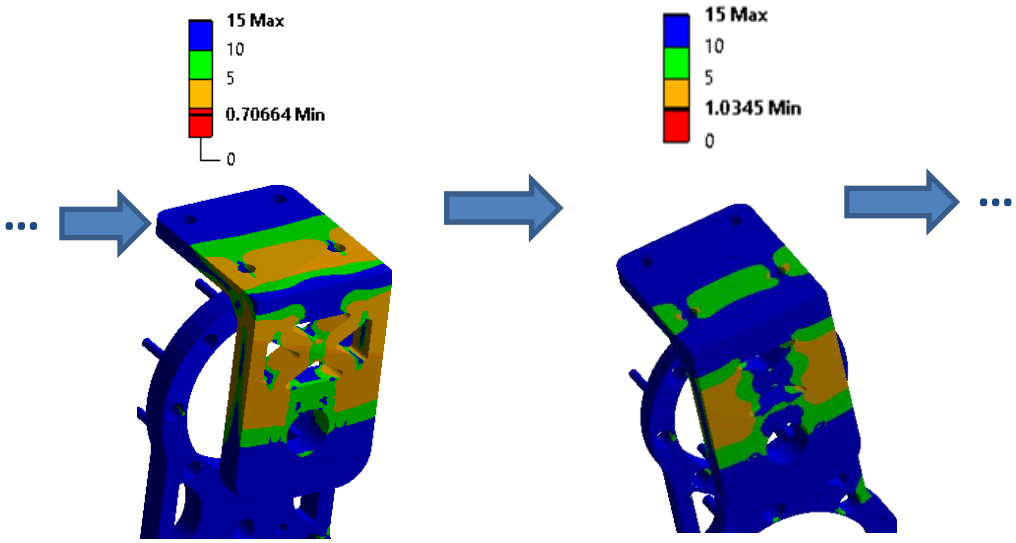

Figure 35. Example FEA Design Iteration (Plotting SF)

The results of the final accepted design for each part are described in the following sections. For changes between each iteration, details can be found in Appendix B.

4.2. Upper Frame FEA

4.2.1. Loading and Boundary Conditions

The location of boundary conditions and applied loads used on the upper frame are shown in Figure 36. The fixed supports restrict motion by setting a displacement boundary condition of zero in all directions along the highlighted surfaces, which is where bolts will be mounted. Moments from the motors, when used, are applied to the frame as shown. The force from the ground reaction force and user's weight is applied to the top bracket.

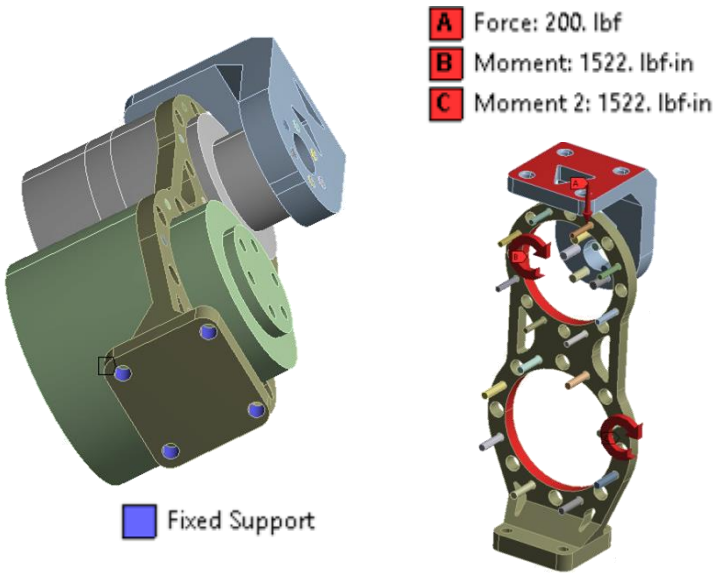

Figure 36. Upper Frame Loads and Boundary Conditions

4.2.2. MESHING

The simplified components in Figure 33 and Figure 36 cannot be fully removed from the analysis because they are used as a means of forces and stresses to travel between components. Dense meshes have been applied to the important structural components with low quality meshes applied to the connecting parts. The mesh for the upper frame analysis runs is shown in Figure 37. Convergence of this mesh is discussed in the results of this and the lower frame runs.

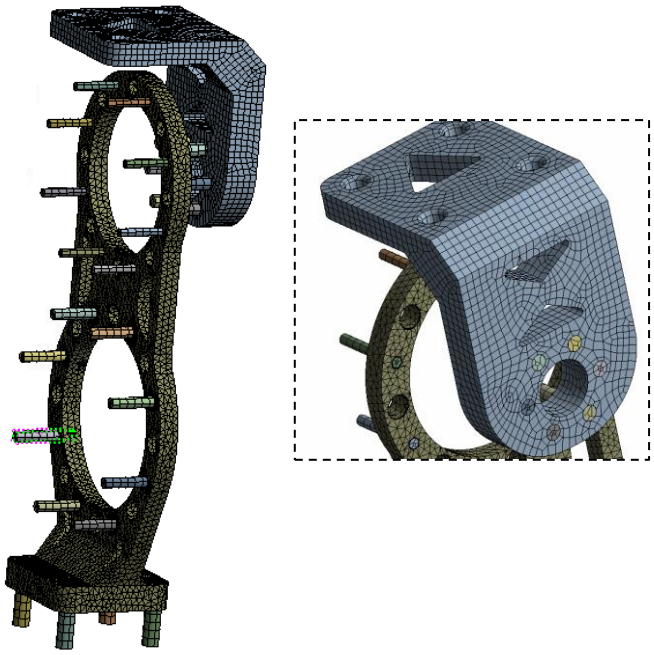

Figure 37. Mesh of Upper Structural Components

4.2.3. LOAD CASES

Two load cases have been applied to the upper frame as indicated.

Load Case 1:

The first load case applied to the upper frame is based on the maximum static forces all applied at once to the frame. The maximum load from walking is 180lbf, obtained from walking ground reaction force data. The maximum torque at the joints is expected to be 172Nm from the inverse dynamics analysis. These loads are applied as shown in Figure 36. Note that this should not occur in reality as the moment does not get applied to the frame in this manner under normal use (the joints move and the motors do not hit peak values at the same time). This load case simulates a case where the leg was

to get “caught” on something in the environment preventing motion which may result in the maximum load from the motors to be applied directly to the frame. The acceptance criteria for this analysis is for the stress to stay below the yield strength of the material. Note diminishing returns has been taken into account when removing material.

Load Case 2:

The second load case applied to the upper frame is a fatigue analysis. The ground reaction force transferring into the prosthetic through an entire walking cycle is shown below in Figure 38. A static analysis has been completed in ANSYS with the maximum expected ground reaction force value of 200lbs repeated through this profile.

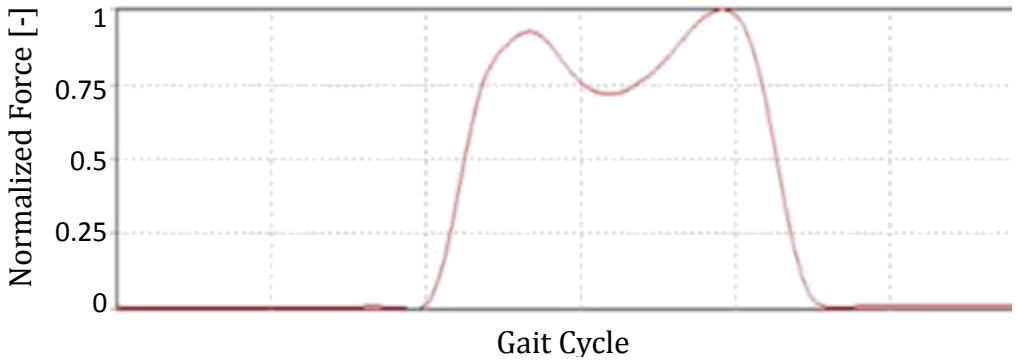

Figure 38. Ground Reaction Force Profile

The fatigue analysis was evaluated using a static analysis of only the force from Figure 36 and not the moments. In a realistic use the moments would not be applied to the frame without the prosthetic getting stuck, so for such a fatigue load case the moments would be absent from those parts. The fatigue life was evaluated using

Goodman mean stress theory with the alternating stress ratio set to semi-log interpolation. The settings for the fatigue analysis are based on best practices for experimental data reported by literature [35-37].

4.2.4. RESULTS & CONVERGENCE

A stress singularity has been identified in a corner of one of the holes as shown in Figure 39, with a large stress value. This phenomenon is similar to that also found in the lower frame, shown by Figure 45 and Figure 46. Upon investigation, the stress here is not an issue and can be neglected. This conclusion was drawn based on the same information presented in the results from the lower frame analysis, which can be referenced for more details on this result. The stress in the remainder of the part is below yield and passes the requirements. Stress elsewhere on the part has also converged. The geometry in Figure 39 has been chosen as the final design for the upper frame.

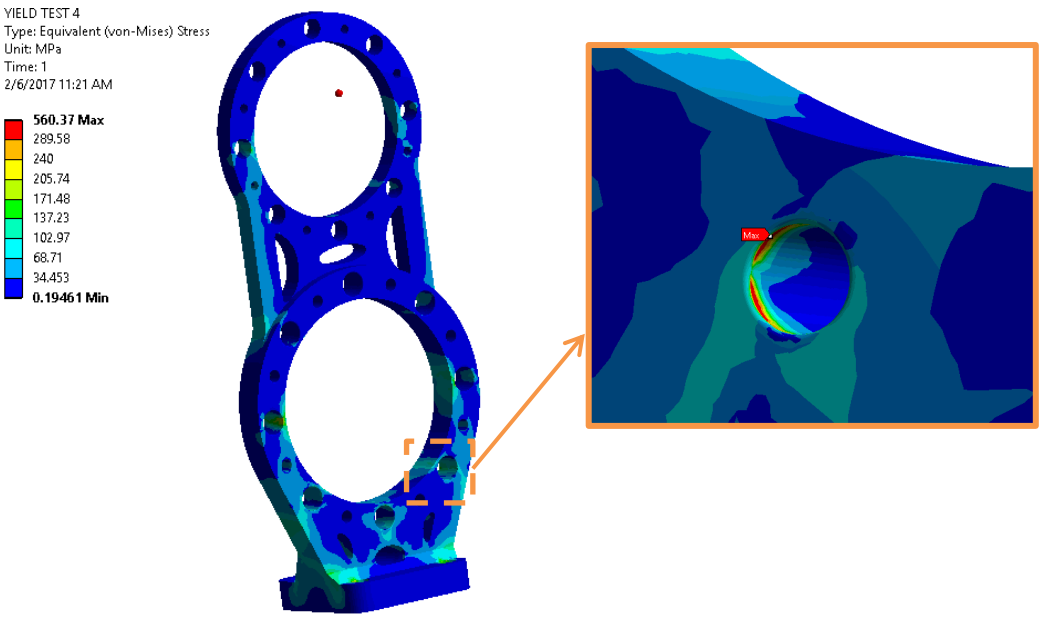

Figure 39. Main Frame Mount FEA, von-Mises Stress

The knee bracket performs well below the yield strength and is arguably overdesigned, as shown in Figure 40. During the design phase several modifications were made and the minimal reduction in mass from further iterations past this final design are not considered worth the computational time for this part. In other words there are no further significant improvements to be made. Hole placement allowed three cuts to be made, one on the top and two on the side. Originally four triangular cuts were planned for side but the part did not pass FEA loads without the extra support.

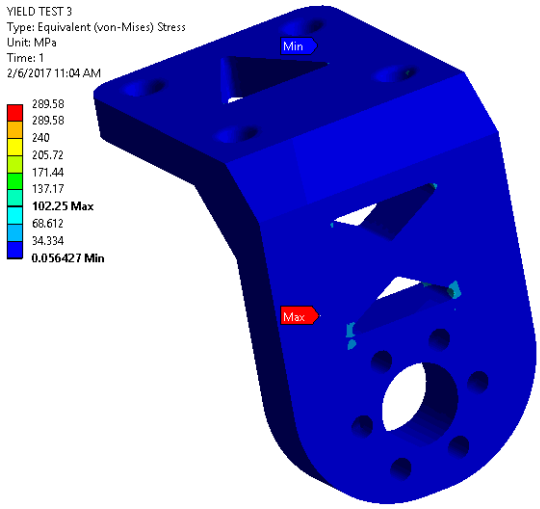

Figure 40. Upper Frame Knee Bracket FEA

The fatigue analysis completed without damage and hit the value for infinite life (the analysis stopped). The results plotting safety factor are shown in Figure 41. As the fatigue analysis does not include the moments, it is not nearly as damaging as the worst case static analysis and is not the limiting factor. Focus for this part as such was not placed on the fatigue analysis. This is a good sign for the design and it has been accepted, but it is also important to note that the design should not be considered safe without physical testing to validate the analysis.

The safety factor for the fatigue results have been plotted in the following figure. The lowest value is shown in the knee bracket, which was one reason for removing the triangular holes from that location during design iterations.

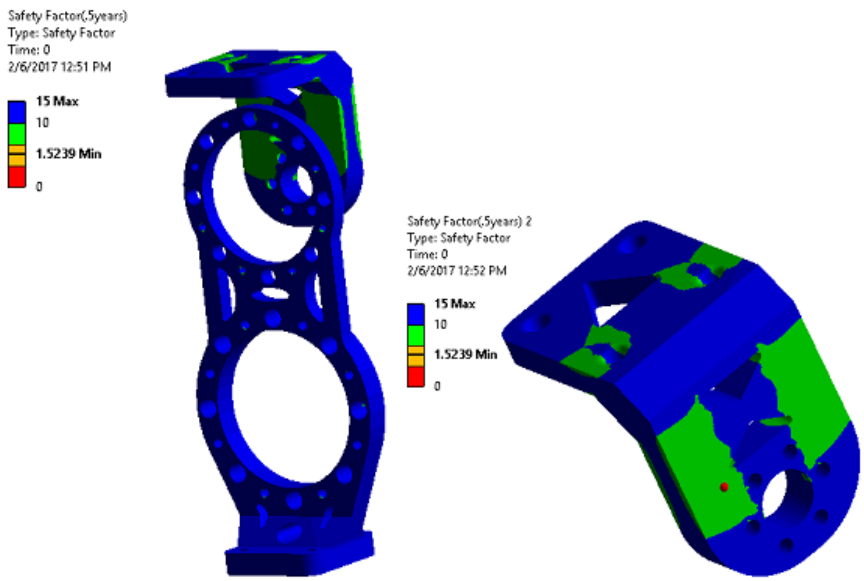

Figure 41. Fatigue SF of Upper Frame

4.3. BOTTOM FRAME

The bottom frame was designed by creating mounting points for identified off-the-shelf brackets and flanges. As it failed initial FEA simulation runs, the shape was modified to be more structurally sound.

4.3.1. LOADING AND BOUNDARY CONDITIONS

The boundary conditions applied to the bottom frame are shown in Figure 42. The fixed support acts as a displacement boundary condition restricting motion in every direction. Stiffness has been set to update each iteration for the analysis runs.

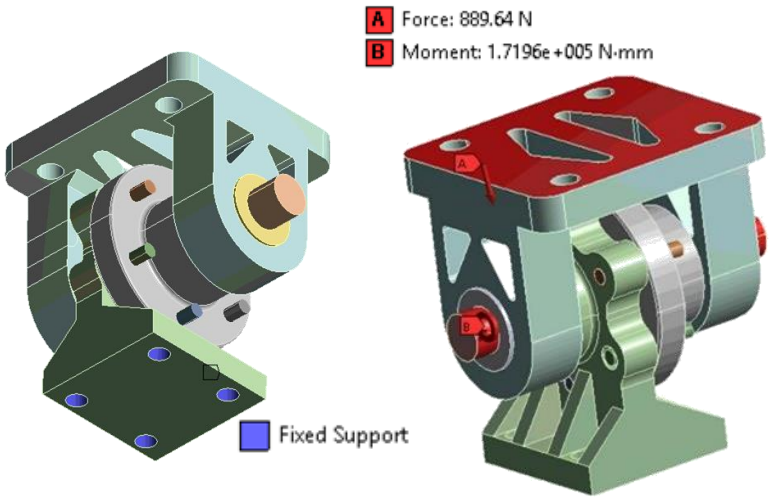

Figure 42. Bottom Frame Loads and Boundary Conditions

The maximum moment possible from the motor has been applied to the shaft as shown in Figure 42. The load transfers to the structural components through connections, which is detailed in Appendix B. The load applied at the top of the bracket is from the ground reaction force.

4.3.2. MESHING

The mesh for the bottom frame is shown in the following figure.

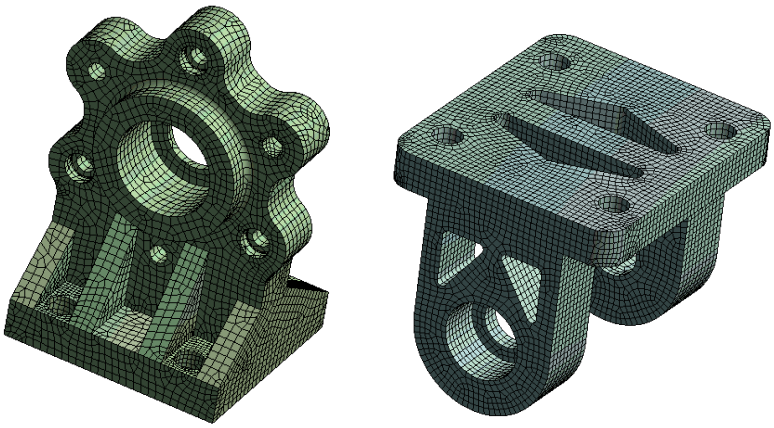

Figure 43. Mesh for Ankle Bracket Structural Parts

Convergence of this mesh is discussed in the results for this part.

4.3.3. LOAD CASES

Load Case 1:

The first load case applied to the lower frame is a static analysis with the forces and moments as shown in Figure 42. The acceptance criteria for the part is to stay below the yield strength when investigating von-Mises, though some minimal reported plastic deformation has been allowed on this part at corners near the bolts, which is considered negligible and discussed in the results.

Load Case 2:

A fatigue analysis with the same loading as described for the upper frame has been applied to the lower frame.

4.3.4. RESULTS & CONVERGENCE

Shown in Figure 44, the final iteration of the upper bracket on the ankle passes the analysis without issue. Taking into account diminishing returns, the part was no longer worth reducing and chosen as shown for the final design. The bottom bracket is weaker, however, and seemingly has some high stress values which warranted further investigation.

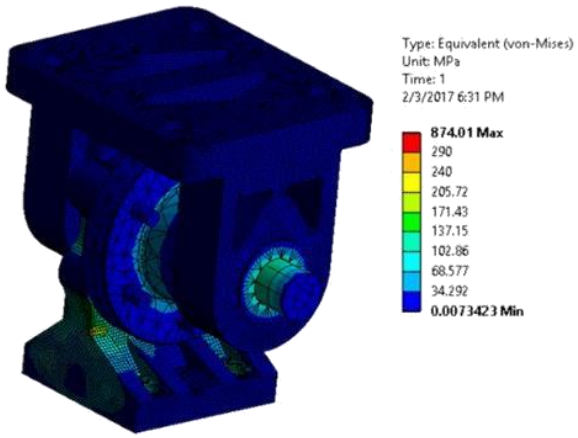

Figure 44. Ankle Load Case 1 FEA Results

The von-Mises stress on the lower bracket from the static analysis is shown in Figure 45. The entire part is below the yield strength with the exception of some corners as shown on the edge of the bolt slots. Upon further investigating this is not considered to be an issue. Allowing some plastic deformation in this small area will not cause any harm to the function of the part, and due to the nature of the analysis the stress in corners is sometimes unavoidable. A small mesh study was also introduced at this corner which suggests the result is a stress singularity. The value here is theoretically infinity. Based

on St. Venant's principle, the stress at this singularity can be neglected [38]. Shown in Figure 45 and Figure 46, the mesh size has been modified from 0.3m, to 0.15m, to 0.05m. The stress in this corner continues to increase with each density increase and does not converge.

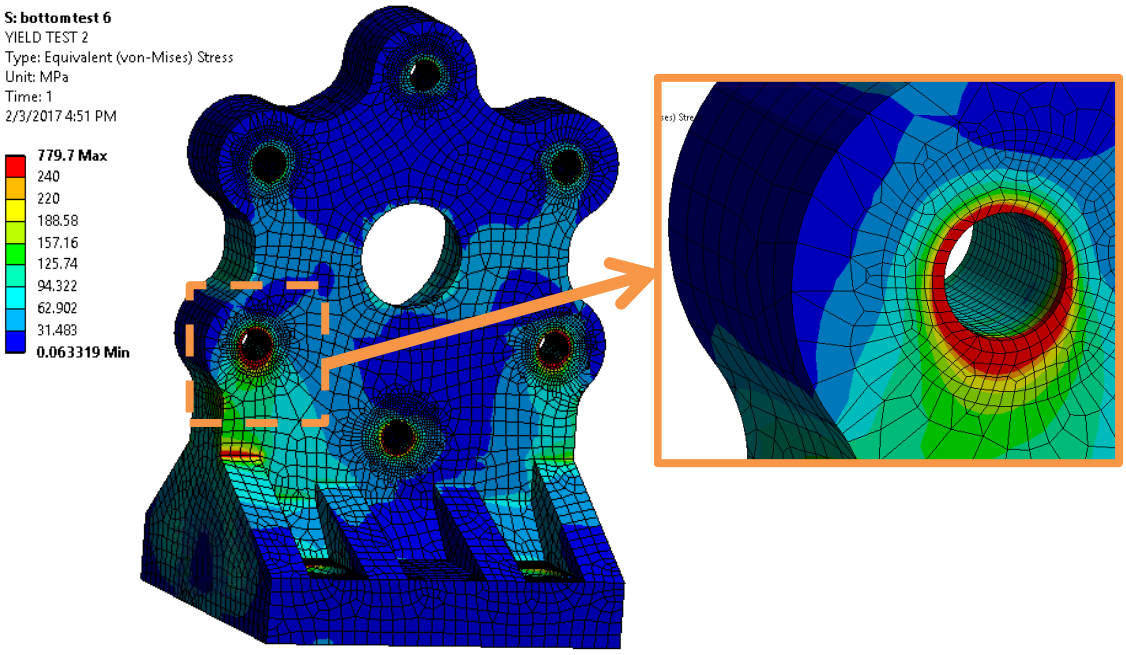

Figure 45. Lower Frame von-Mises Stress, Static Analysis

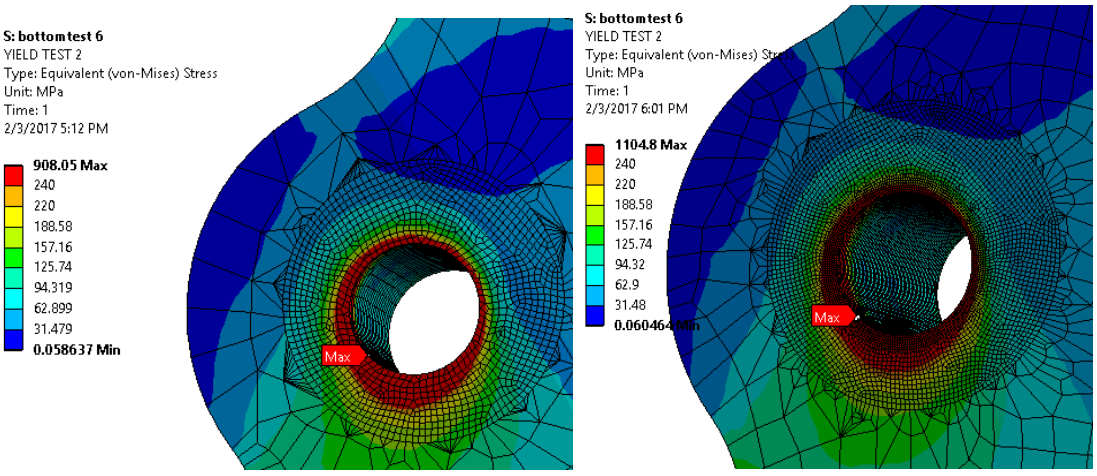

Figure 46. Stress Singularity at Corner

As described for the upper frame analysis, the fatigue analysis for the lower frame has been applied with the force profile repeated but without the moment. A life analysis results in infinite life for both parts suggesting the parts will not fail in fatigue. A safety factor of continuous use for 0.5 years has also been applied with no issues found on these parts, shown in

Figure 47.

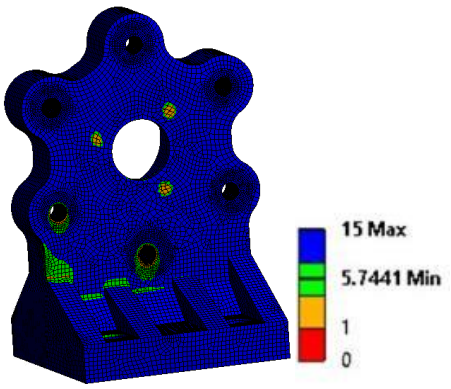

Figure 47. Ankle Bracket Fatigue Safety Factor

4.4. RSEA

Many concept shapes have been tested for the RSEA torsional spring. Shapes are based on those from published literature with modifications to meet the custom spaces needed here. For material, initially aluminum was planned due to its modulus and costs. However, very large deflections are required in a small space with extremely high stress as a result. Upon further literature reviews, the high stress values have been unavoidable and stronger material such as steel alloys are used for these springs. Marging Steel 300 has been selected based on its high strength and successful use in other RSEA torsional spring designs from literature [39]. The material has a yield strength of 2 GPa and a modulus of 193 GPa.

4.4.1. Loading and Boundary Conditions

The loads to the RSEA spring disk are shown in Figure 48. The inner holes are fixed with a moment applied on the outer surface.

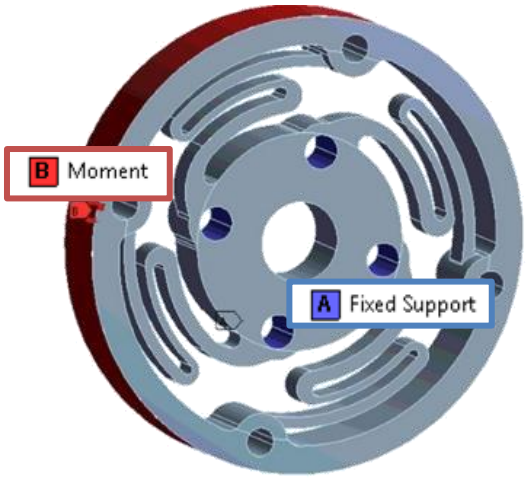

Figure 48. RSEA Spring Disk Loads and B.C.

4.4.2. MESHING

An example of the mesh used for the RSEA is shown below. Design variations changed the mesh as the shape changed, but sizing has stayed consistent with that shown in Figure 49.

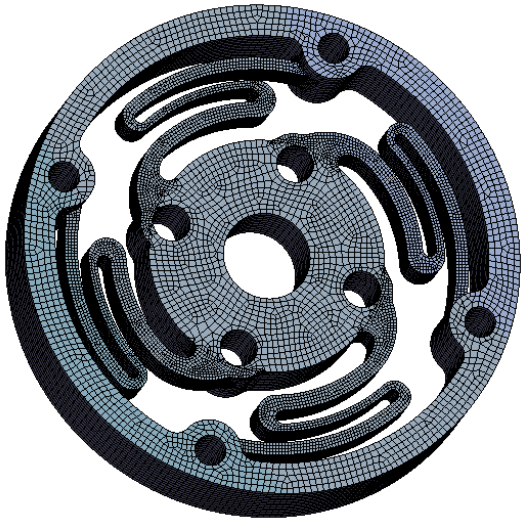

Figure 49. RSEA Mesh

4.4.3. LOAD CASES

The RSEA spring has been loaded in a single static analysis with conditions as shown in Figure 48. The designs have been iterated until a moment load of 172Nm results in a deflection of near 5 degrees on the outer edge. Several iterations have been run with large deflection turned on to take into account nonlinear calculations, but with linear elastic properties to speed up the iteration times. Other iterations have been run in a fully nonlinear elastic-plastic analysis. In such cases, two steps are applied. Starting at zero load, step 1 applies a load and step 2 removes it. Using the two steps any plastic deformation of the spring can be investigated.

4.4.4. RESULTS

Initial concept shapes of perpendicular loops using aluminum flexed and deformed well but suffer from high stresses. Several iterations were performed at an attempt to optimize this shape but the stress values remained too high. Other shapes flexed with less stress and withstood higher loads, so this design shape has been scrapped.

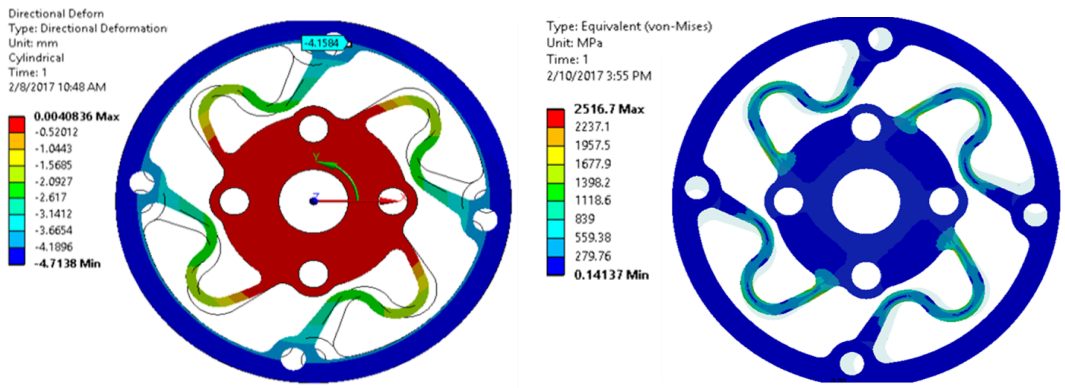

Figure 50. RSEA Results for Perpendicular Loop Concept

Following other concepts from literature, parallel loops seem typical to performing well with lower stress [17, 39]. Tested concepts with parallel loops include 3 loops with the connecting ends 90 degrees apart, 4 loops with the connecting ends at the same angle, and a larger disk with 5 loops connecting 90 degrees apart. Each of these parallel loop design concepts has also been iterated to find the optimum dimensions.

Shown in Figure 51, the parallel concept with 3 loops has been successfully iterated to a deflection of around 5 degrees. Changes in iterations were unable to get the von-Mises stress significantly below the yield at some extreme points on the edges. These high values only occur at infinitesimally small points on the edges and as shown from the stress plot the flexing loops appear acceptable, though this did prompt an elastic-plastic analysis to investigate any potential plastic deformation, described below. This image is from an elastic analysis with large deflection (nonlinearities) turned on.

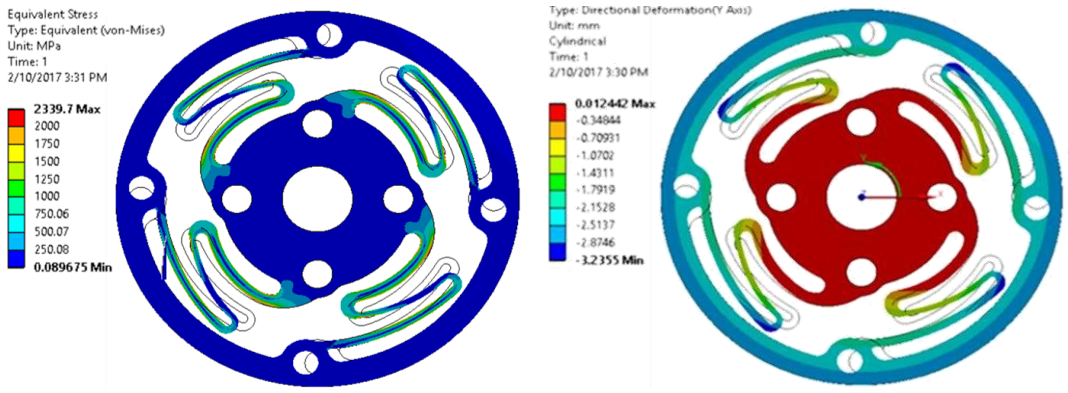

Figure 51. RSEA Spring Disk Concept – Three Parellel Loops

The concept from Figure 51 was also placed in a fully non-linear elastic-plastic analysis with large deflection to investigate the high stress values. The loaded and then unloaded deformation is plotted below.

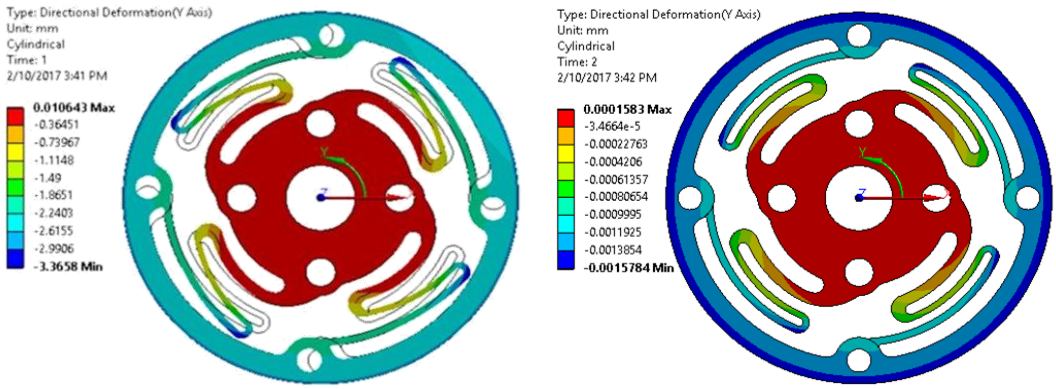

Figure 52. Elastic-Plastic Results Showing No Plastic Deformation

From the elastic-plastic analysis, no noticeable permanent deformation was found. The disk was cycled in the loading without issue. The stress in the loop is shown in the following figure, with red indicating material that is past the yield point. The stress values increase near some of the edges as mentioned, but the material is performing

acceptably with no visible areas of significant concern and no plastic deformation that impacts performance of the analysis.

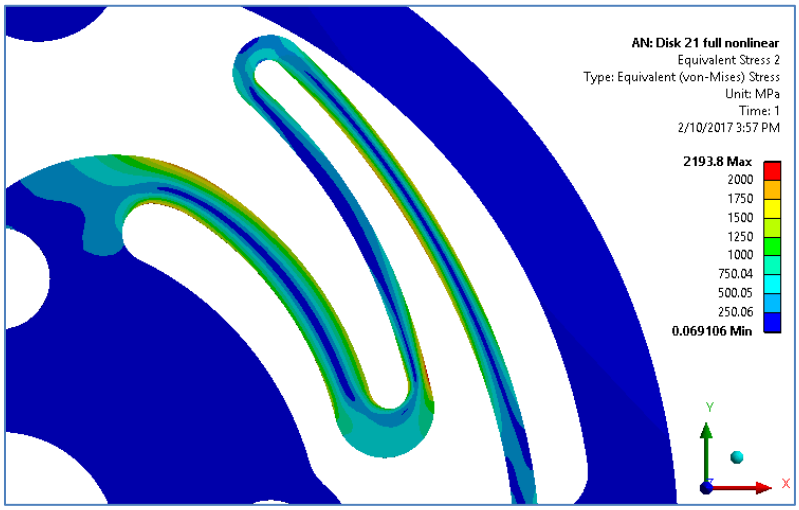

Figure 53. Elastic-Plastic Analysis Stress Results

Results from the parallel concept with 4 loops are shown in the following figure. Through iterations, no clear benefit was found to the extra loop compared to the three loop version.

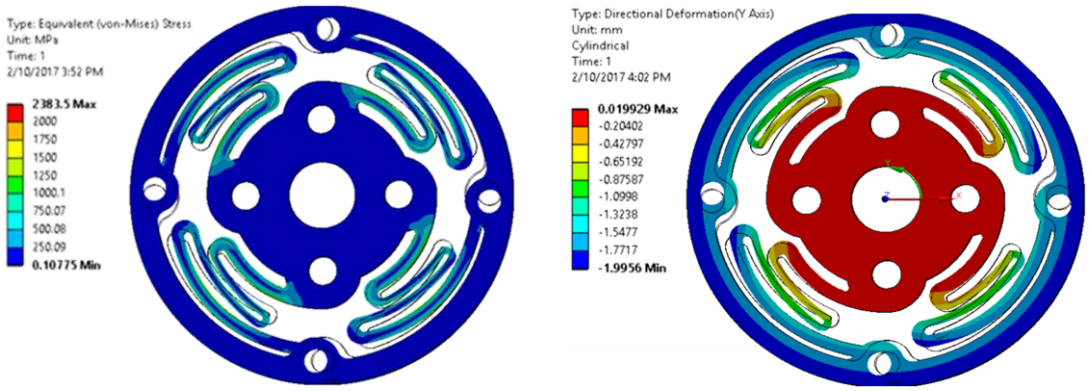

Figure 54. RSEA Disk - Four Parallel Loops

The results of the disk with five loops is shown in Figure 55. The stress and deflection remained largely the same compared to the three and four loop designs. By iterating fillet shapes in the corners where a stress concentration appeared to occur, the maximum von-Mises was lowered below yield. This maximum appears to be a singularity with values immediately close to it dropping significantly in magnitude. This final version performs below the yield of the material, but if the disk is overloaded the resulting type of plastic deformation is still not expected to be an issue, as was shown by an earlier design in Figure 52.

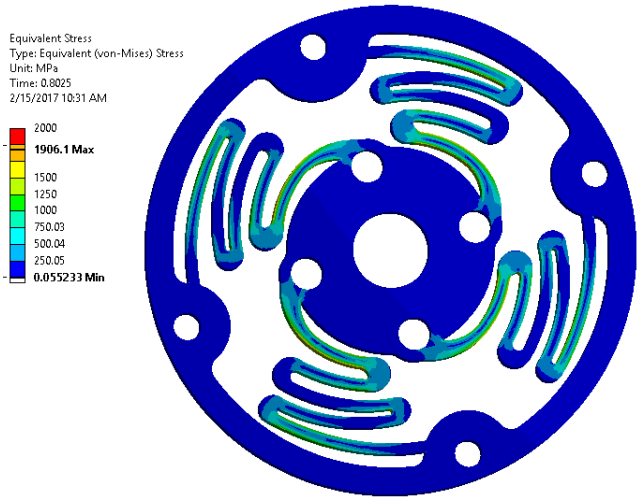

Figure 55. Final RSEA Disk Stress

The circumferential deflection of the final design is plotted in Figure 56. This value results in deflection of 5.2°.

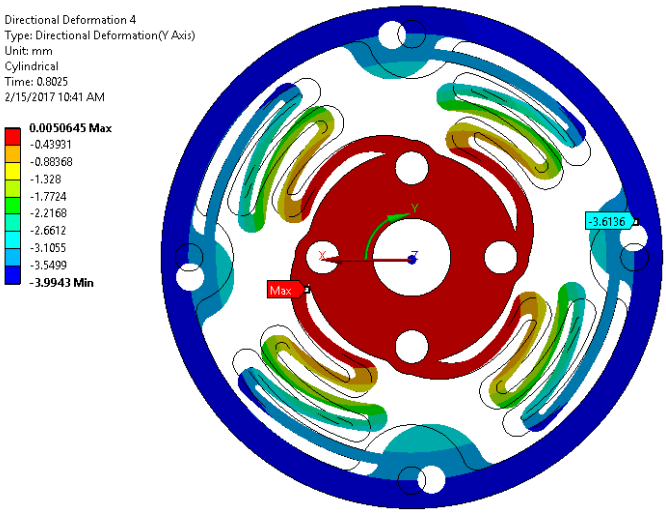

Figure 56. Final RSEA Disk Deflection

The connecting disk that holds the pulley to the spring has also been tested. The intent of this part is to stay below yield and not deform while connecting a pulley. Shown below, using standard aluminum the part is well below the yield strength and no circumferential deflection occurs.

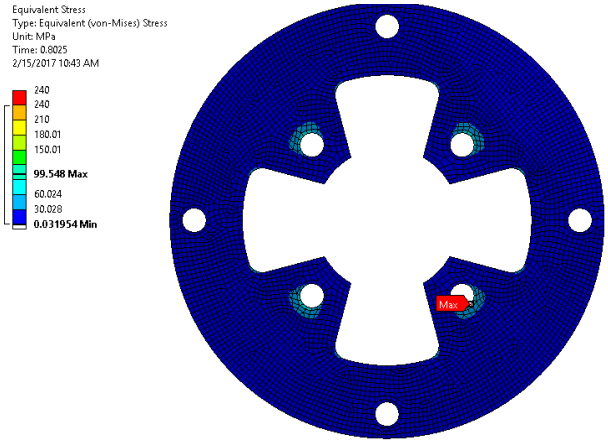

Figure 57. RSEA Connecting Disk FEA Results

4.4.5. CONVERGENCE

A mesh convergence study has been completed on the torsional spring. Mesh size was decreased along only the deflecting areas of interest at sizes that become computationally costly. It was sized as low as 0.25mm; anything lower required more memory than available in the machine and was unable to complete. Images of the meshes studied are shown in Figure 58.

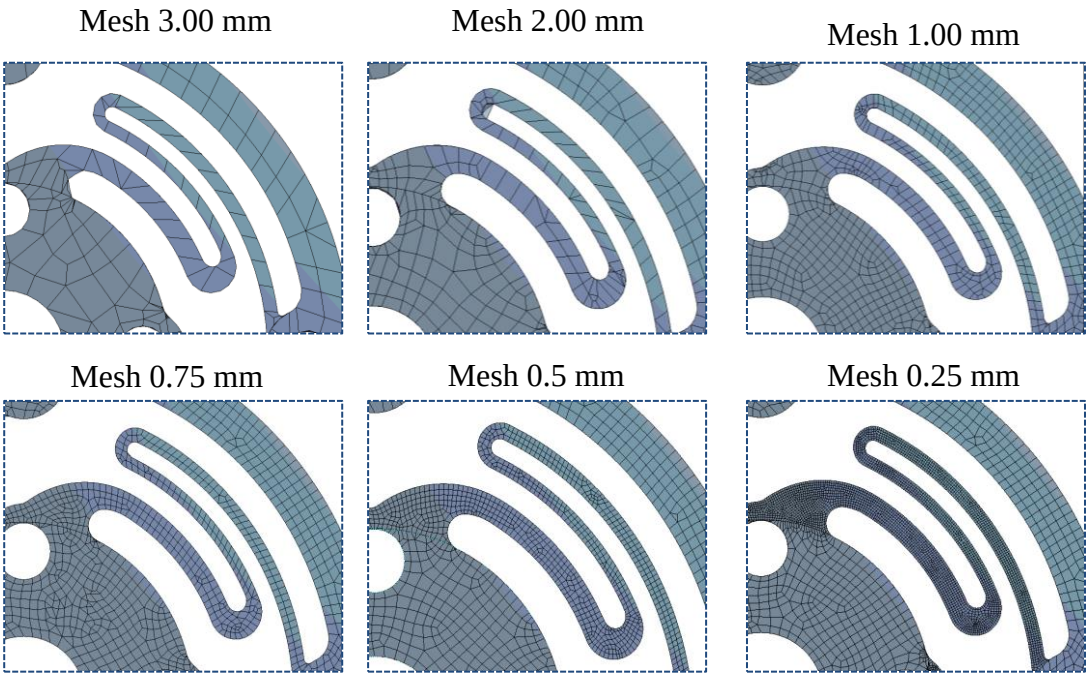

Figure 58. RSEA Mesh Convergence Study

A graph showing the convergence of the mesh size of the disk is shown in Figure 59. As mentioned, computational limitations prevented the mesh size from being lowered any further. Measuring the deflection of the disk was the major point of the analysis and did not require a dense mesh for accuracy, as shown by the graph. This convergence study was performed on the disk with three parallel loops and results held valid for all versions of the disk with smaller studies completed for the other versions.

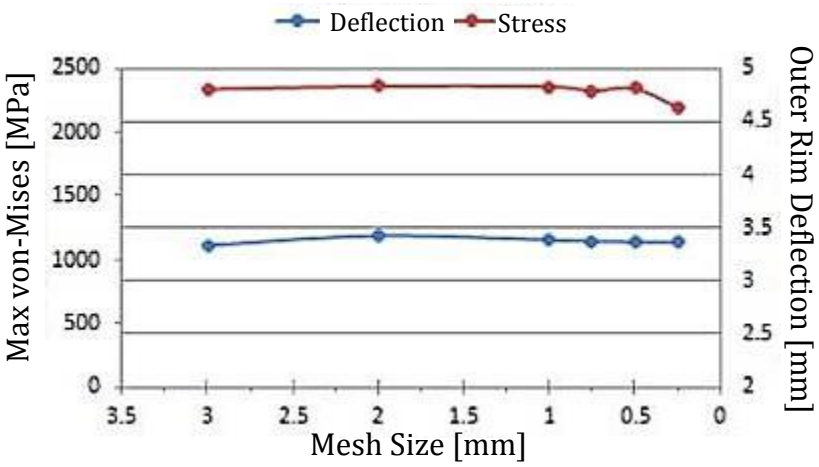

Figure 59. Mesh Convergence

5. HARDWARE, MANUFACTURING, AND ASSEMBLY

Parts are purchased off the shelf when possible. This includes the motors, pyramid adapters, adjustable pylon, timing belt pulleys, the flexible foot, tensioner support bearing, general bearings, and the flanges and supports. The frame components and RSEA are to be machined from stock metal. Aluminum is used for all metal components excluding the RSEA spring, which is to be made from Marging Steel 300. For this thesis the frame has been 3D printed for an initial prototype display. The tensioner bracket, RSEA pulley, and tensioner pulley are also to be 3D printed but with stronger materials, such as printed metal, for the final version. The harmonic drives have been custom ordered for this application. Structural components are being machined based off of CAD files with drawings created for details and notes. Drawings for the initial prototype are shown in Appendix C.

The hardware for the ankle has been chosen to ensure the part survives large torques. In many cases on other prosthetics, such as with AMPRO II, shafts are secured with setscrews. In this case the gearing stage takes place before the shaft on the ankle, however, so slipping is more of a possibility. A keyed shaft and flange have thus been chosen on the ankle as shown in the exploded view of Figure 60.

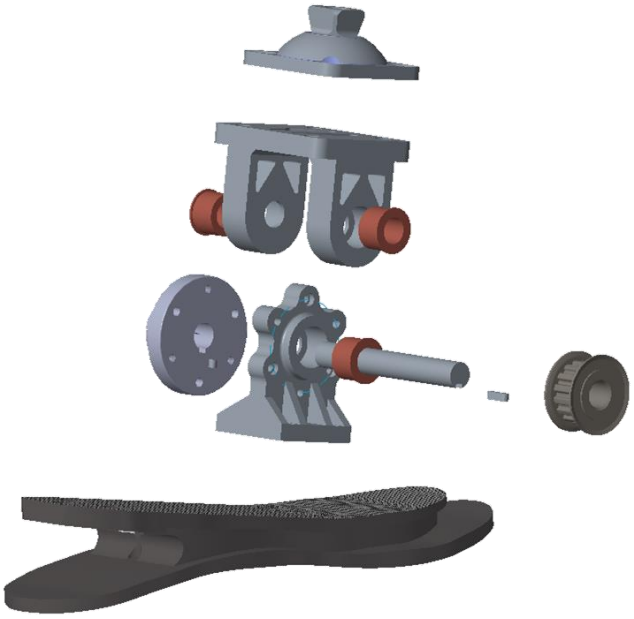

Figure 60. Ankle Design Exploded View

All hardware is standard off-the-shelf components. An example of how the hardware connects the upper assembly is shown in Figure 61.

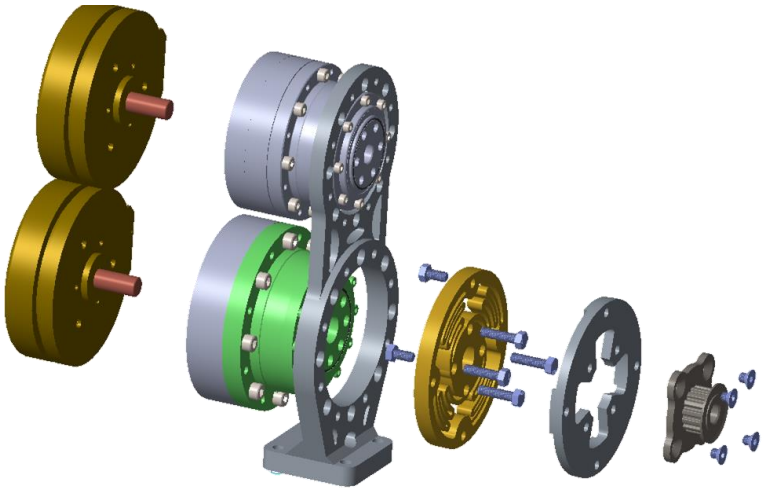

Figure 61. Upper Frame Exploded View

6. RESULTS

6.1. FINAL DEVICE DESIGN

The proposed device being built for this thesis is shown in Figure 62. Improvements compared to AMPRO II include adjustable height, functionality on both legs, a flexible foot, lighter (it is estimated to be 20% lighter), modularity, and it is capable of using elastic components for energy reduction. The elastic energy reduction components include springs that apply a constant torque at the ankle and a RSEA that is designed for reducing power requirements rather than torque control. To reduce risk, new elastic element concepts are optional additions and not built permanently into the device. This allows modifications and testing both with and without each concept.

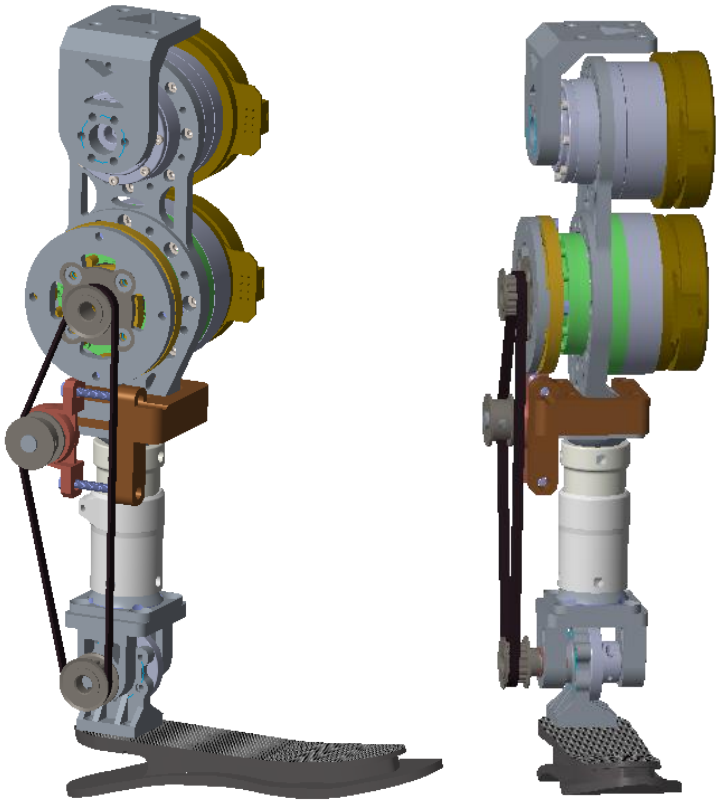

Figure 62. Proposed Device

Component details are shown in Figure 63.

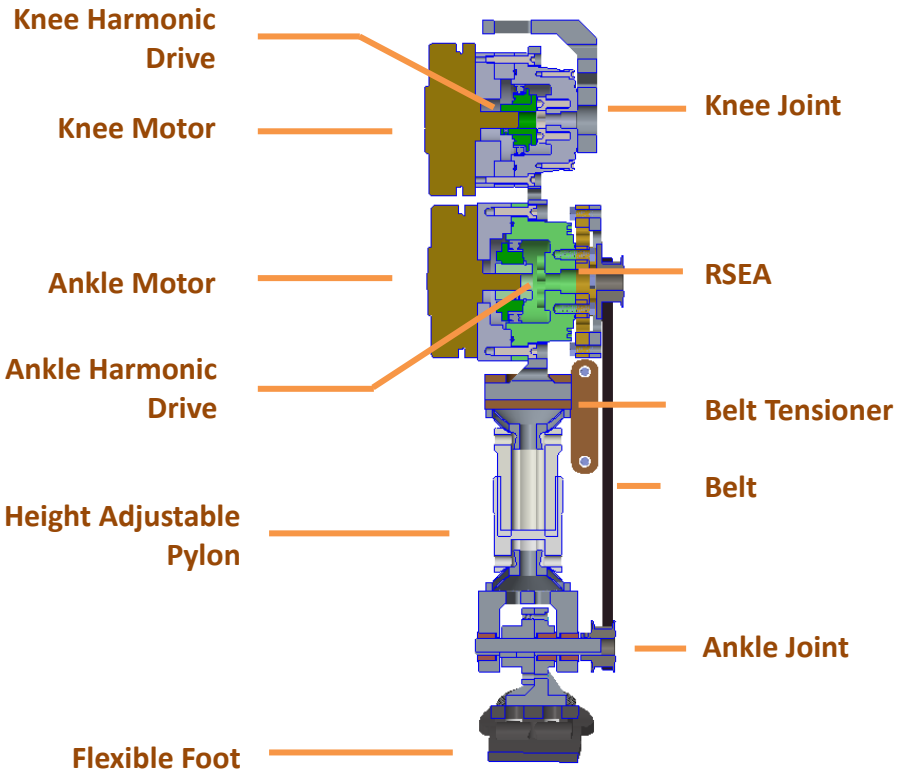

Figure 63. Prosthetic Part Diagram

6.2. FUTURE WORK

Due to the magnitude of this project, research will continue on the prosthetic past this M.S. work and will likely involve additional students in the future. Initial thoughts on a continued future work schedule are shown in the following table. This is subject to change. Work must include electronic design, controls design, and testing.

Table 1. Schedule of Continued Project Work

ITEM	START	END	STATUS
Complete Design of Optional Components/Add-ons			
	April 2017	August 2017	In Progress + Future Work
Electronics Design			
		April 2018	Future Work
Controller Design			
		April 2018	Future Work
Testing with Humans and Comparison to AMPRO II			
		May 2018	Future Work

6.3. IMPACT OF THESIS

Currently, only two powered lower limb prosthetics are commercially available on the market. Rejection rates with prosthetic products are also unacceptably high [40, 41]. The high mass and lack of functionality leaves patients wanting more. Simply put, the burden of using many prosthetic devices are often not worth the limited improvement in functionality they provide. This shows a significant gap and need in the market for improved devices such as that which will be possible with this research.

The device that has been developed in this thesis provides numerous methods to reduce the required power of the motors which can be used to significantly reduce energy requirements, electronics, motor size, etc. After a proof of concept is finalized through testing, this stands to significantly reduce energy expenditure of the user over currently marketed devices by creating a lightweight powered prosthetic. The device is also adjustable and modular to reduce both cost and time needed for customization to different patients.

7. CONCLUSIONS

Several new design concepts have been investigated and implemented. Requirements generated through an inverse dynamics analysis indicate restricting and large torque requirements for the ankle. The requirements at the knee did not pose any major design problems. An estimated worst cast requirement of 172Nm is estimated for the ankle torque of a 200lb user. In generating this torque, an optimizer was successfully created for part selection but unable to find a solution. This suggests the need for a trade-off or an alternative means of creating and storing energy to reach the worst case power requirements at the ankle. To finish the actuator design, the requirements were relaxed and changed from the theoretical worst case values to measured values from a physical test of human data. For this case the optimizer was able to find a solution using flat motors and harmonic drives.

Many passive spring design concepts have been investigated through simulations and show potential to reduce the requirements of the actuator. From the simulated concepts, the pre-loaded ankle spring design and RSEA were chosen for further testing and prototyping. The other concepts discussed and evaluated, such as pre-loaded springs in the foot, are also worth future consideration. For this thesis those other concepts were not concluded to be as beneficial as the chosen concepts, however, so they have been omitted from the first prototyping phase to keep the prototyping scope realistic. Future work should consider such concepts.

Modularity has been identified as key design criteria. AMPRO II is only useable by a very small portion of the population. This restricts use both for research and rehabilitation. With that in mind, the new prosthetic is designed to be adjustable with interchangeable components. From a research standpoint, testing some of the more risky concepts such as the pre-loaded ankle springs will greatly benefit from the modularity. Multiple spring stiffness values can be tested and if results are not desirable the springs can be removed altogether. Likewise, the new spring design in the RSEA can be changed to adjust stiffness for testing or even completely omitted.

The final product is shown in Figure 62 and Figure 63. Compared to AMPRO II, it is estimated to be 20% lighter, modular, adjustable, capable of multi-contact walking, etc. The overall benefits of this design for both rehabilitation and research use are vastly improved. Future work will continue as outlined in the results. Initially, the electronics and controls must be designed and implemented. Additional concepts considered here but not chosen to be built with the initial prototype can also be investigated as future work. Ultimately, all of these concepts will need human testing to measure energy expenditure. A significant gap exists in the market for a good lower limb powered prosthetic and this device holds potential to fill that gap.

REFERENCES

[1] K. L. Owings M, "Ambulatory and Inpatient Procedures in the United States, 1996," in *National Center for Health Statistics*, C. f. D. C. a. P. U.S. Dept. of Health and Human Services, Ed., ed. Hyattsville, Md., 1998.

[2] H. A. V. Frank Sup, Jason Mitchell, Thomas J. Withrow, Michael Goldfarb, "Preliminary Evaluations of a Self-Contained Anthropomorphic Transfemoral Prosthesis," *IEEE Transactions on Mechatronics*, vol. 14, pp. 667-676, 2009.

[3] Ossur. (2017, January 2). *Power Knee* [Catalog]. Available: https://www.ossur.com/prosthetic-solutions/products/dynamic-solutions/power-knee

[4] S. Patric, "Bionmechanical Analysis of Lower Limb Powered Prosthesis," M.S. Thesis, Dept. Mech. Eng., Texas A&M University, College Station, TX, 2016.

[5] E. C. Martinez-Villalpando, Mooney, L., Elliott, G., & Herr, H., "Antagonistic Active Knee Prosthesis. A Metabolic Cost of Walking Comparison With a Variable-Damping Prosthetic Knee," in *33rd Annual Inernational Conference of the IEE EMBS*, Boston, MA, 2011, pp. 8519-8522.

[6] D. A. Winter, "Moments of Force, Mechanical Power in Jogging," *Journal of Biomehcanics*, vol. 16, pp. 91-97, 1983.

[7] Kota Z. Takahashi a, Steven J. Stanhope, "Mechanical energy profiles of the combined ankle–foot system in normal gait: Insights for prosthetic designs," *Gait & Posture*, vol. 38, pp. 818-823, September 2013 2013.

[8] F. B. Roberta Alo, Giacomo Mantriota, "An Innovative Design of Artificial Knee Joint Actuator With Energy Recovery Capabilities," *Journal of Mechanisms and Robotics*, vol. 8, pp. 1-8, 2016.

[9] R. I. Kevin W. Hollander, Thomas G. Sugar, Donald Herring, "An Efficient Robotic Tendon for Gait Assistance," *Journal of Biomechanical Engineering*, vol. 128, pp. 788-791, 2006.

[10] G. J. Flynn L, Limenez-Fabian R, Vanderborght B, Vitiello N, Lefeber D, "Ankle–knee prosthesis with active ankle and energy transfer: Development of the CYBERLEGs Alpha-Prosthesis," *Robotics and Autonomous Systems*, vol. 73, pp. 4-15, 2015.

[11] L. J. Kim HG, Jang J, Park S, Han C, "Design of an Exoskeleton with Minimized Energy Consumption based on using Elastic and Dissipative Elements," *International Journal of Control Automation and Systems,* vol. 13, pp. 463-474, 2015.

[12] L. M. M. Elliott J. Rouse, Ernesto C. Martinez-Villalpando and Hugh M. Herr, "Clutchable Series-Elastic Actuator: Design of a Robotic Knee Prosthesis for Minimum Energy Consumption " in *IEEE International Conference of Rehabilitation Robotics*, 2013, pp. 1-6.

[13] L. M. a. H. Herr, "Continuously-Variable Series-Elastic Actuator," in *IEEE International Conference on Rehabilitation Robotics*, Seattle, WA, 2013.

[14] V. G. Pierre Cherelle, Arnout Matthys, Bram Vanderborght, and Dirk Lefeber, "Design and Validation of the Ankle Mimicking Prosthetic (AMP-) Foot 2.0," *IEEE Transactions on Neural Systems and Rehabilitation Engineering,* vol. 22, pp. 138-148, 2014.

[15] Q. L. M. Donald, "Design and Performance Evaluation of a Rotary Series Elastic Actuator," in *International Conference on Intelligent Robotics and Applications*, Montreal, QC, Canada, 2012, pp. 555-564.

[16] G. C. Giorgio Carpino, Fabrizio Sergi, Nevio Luigi Tagliamonte, Eugenio Guglielmelli, "A Novel Compact Torsional Spring for Series Elastic Actuators for Assistive Wearable Robots," *Journal of Mechanical Design,* vol. 134, pp. 1-10, 2012.

[17] C. F. Henry Phalen, Marci Carter. (2017, January 24). *The Incorporation of a Rotary Series Elastic Actuator in a Hybrid Neuromuscluar Stimulation System* [Online]. Available: www.engineering.pitt.edu/Sub-Sites/Labs/Sharma-Lab/_Library/Spring2014_2/

[18] C. T. Biddiss E, "Dielectric elastomers as actuators for upper limb prosthetics: Challenges and opportunities.," *Medical Engineering & Physics* vol. 30, pp. 403-418, 2008.

[19] B. E. L. Amanda H. Shultz, Michael Goldfarb, "Running With a Powered Knee and Ankle Prosthesis," *IEEE Transactions on Neural Systems and Rehabilitation Engineering,* vol. 23, pp. 403-412, 2015.

[20] A. A. S. Albert E. Yousif, "The Design, Development and Construction of an Adjustable Lower Extremity," *IOSR Journal of Engineering,* vol. 2, pp. 30-42, 2012.

[21] I. P. Daniel Rihs. (2001, 2016, March 1). *Prosthetic Foot Design* [Online]. Available: www.monash.edu.au/rehabtech/research/reports/FEETMAST.PDF

[22] J. E. M. Brian E. Lawson, Don Truex, Amanda Shultz, Elissa Ledoux, and Michael Goldfarb, "A Robotic Leg Prosthesi, Design, Control, and Implementation," *IEEE Robotics & Automation Magazine,* vol. 21, pp. 70-81, 2014.

[23] A. B. Frank Sup, Michael Goldfarb, "Design and Control of a Powered Knee and Ankle Prosthesis," in *IEEE International Conference on Robotics and Automation*, Roma, Italy, 2007, pp. 4134-4139.

[24] A. D. Ames, "Human-Inspired Control of Bipedal Walking Robots," *IEEE Transactions on Automatic Control,* vol. 59, pp. 1115-1130, 2014.

[25] A. Ames, Galloway, K., & Grizzle, J., "Control Lyapunuv Functions and Hybrid Zero Dynamics," in *IEEE 51st Annual Conference on In Deciscion and Control*, 2012, pp. 6837-6842.

[26] W. H. V. Paredes, S. Patric, P. Hur, "Upslope Walking with Transfemoral Prosthesis using Optimization based Spline Generation," in *IEEE/RSJ International Conference on Intelligent Robotics and Systems*, Daejeon, Korea, 2016, pp. 3204-3211.

[27] C. L. Vaughan, Davis, B.L., *Dynamics of Human Gait*, 2 ed. Cape Town, South Africa: Human Kinetics Pub, 1992.

[28] K. L. C. Erik B. Simonsen, Ragnhild I Skorini, Peter K. Larsen, "Explanations Pertaining to the Hip Joint Flexor Moment during the Stance Phase of Human Walking," *Journal of Biomechanics*, vol. 28, pp. 542-550, 2012.

[29] D. G. T. C. David Remy, "Optimal Estimation of Dynamically Consistent Kinematics and Kinetics for Forward Dynamic Simulation of Gait," *Journal of Biomechanical Engineering*, vol. 131, pp. 1-9, 2009.

[30] D. A. Winter, "Kinetics: Forces and Moments of Force," in *Biomechanics and Motor Control of Human Movement*, 2nd ed: Wiley-Interscience, 1990, pp. 75-102.

[31] M. L. M. Dennis E. Andersona, Maury A. Nussbaum, "Maximum Voluntary Joint Torque as a Function of Joint Angle and Angular Velocity: Model Development and Application to the Lower Limb," *JOURNAL OF BIOMECHANICS*, vol. 40, pp. 3105–3113, 2007.

[32] D. A. Winter, "Kinematic and Kinetic Patterns in Human Gait: Variability and Compensating Effects," *Human Movement Science 3*, pp. 51-76, 1984.

[33] MoogComponentsGroup. (2017, January 2). *BN23 Specifications* [Online]. Available: http://www.moog.com/literature/MCG/BN23-BrushlessDCMotorsDtS.pdf

[34] J. R. Rinderle, "Brushless D.C. Motors and Servo Amplifiers," in *UMass Amherst, Machine Component Design*, U. o. M. Amherst, Ed., 1 ed, 2001.

[35] P. E. Raymond L. Browell, Al Hancq, "Predicting Fatigue Life with ANSYS Workbench: How To Design Products That Meet Their Intended Design Life Requirements " in *International ANSYS Conference*, Pottsburgh, PA, 2006.

[36] R. Browell. (2016, December 1). *Calculating and Displaying Fatigue Results* [Online]. Available: http://ansoft.com/staticassets/ANSYS/staticassets/resourcelibrary/whitepaper/fatigue.pdf

[37] D. A. Hancq. (2016, December 1). *Fatigue Analysis Using ANSYS* [Online]. Available: http://www.ewp.rpi.edu/hartford/~ernesto/F2006/MEF2/Programs/Z-Links/Papers/Hancq.pdf

[38] M. Acin. (2016, December 5). *Stress singularities, stress concentrations and mesh convergence* [Online]. Available: http://www.acin.net/2015/06/02/stress-singularities-stress-concentrations-and-mesh-convergence/

[39] G. C. Dino Accoto, Fabrizio Sergi, Nevio Luigi Tagliamonte, Loredana Zollo, Eugenio Guglielmelli, "Design and Characterization of a Novel High-Power Series Elastic Actuator for a Lower Limb Robotic Orthosis," *International Journal of Advanced Robotic Systems*, vol. 10, pp. 1-12, 2013.

[40] D. T. Pezzin LE, MS EJM, Ephraim P, Rossbach P "Use and Satisfaction With Prosthetic Limb Devices and Related Services," *Archives of Physical Medicine and Rehabilitation*, vol. 85, pp. 723-729, 2004.

[41] D. B. Elaine Biddiss, Tom Chau, "Consumer Design Priorities for Upper Limb Prosthetics," *Disability and Rehabilitation: Assistive Technology* vol. 2(6), pp. 346-357, 2007.

APPENDIX A: MOTOR OPTIONS

Table 2. Motor Options

	BN23-18MG-01	BN23-18MG-02	BN23-23MG-01	BN23-23MG-02	BN23-28MG-01
No load speed [RPM]	9100	9700	8100	8800	7300
Kt (torque constant) [Nm/amp]	0.024	0.035	0.027	0.038	0.03
Torque Gradient [rpm/oz-in]	88.9	90.6	50.6	49.6	39.9
Power Rating [Watts]	142	154	181	210	194
Current Rating [Amps]	7.75	5.43	9.47	7.44	10.45
Voltage [V]	24	36	24	36	24
Cont/Intermittent [rpm/oz-in]	(30, 6400)	(30, 7000)	(40, 6000)	(42, 6800)	(49, 5300)
Intermittent [rpm/oz-in]	(67, 3100)	(67, 3700)	(90, 3500)	(95, 4000)	(110, 3000)
Terminal resistance [ohms]	0.246	0.507	0.178	0.347	0.181
continuous stall [oz-in]	30.7	31.4	42.8	44.7	50.4
intermittent estimate [oz-in]	66	68	91	96	102

	BN23-28MG-02	BS23-18HP-01	BS23-23HP-01	BS23-23HP-02	BS23-23HP-03
No load speed [RPM]	7500	3500	4300	5000	5500
Kt (torque constant) [Nm/amp]	0.044	0.064	0.051	0.066	0.083
Torque Gradient [rpm/oz-in]	36.8	14.7	8.5	8	8
Power Rating [Watts]	215	71	119	131	137
Current Rating [Amps]	7.66	3.7	5.9	4.3	3.3
Voltage [V]	36	24	24	36	36
Cont/Intermittent [rpm/oz-in]	(52, 5600)	(32, 3000)	(40, 4000)	(38, 4800)	(38, 4800)
Intermittent [rpm/oz-in]	(115, 3100)	(71, 2500)	(90, 3500)	(82, 4500)	(82, 4500)
Terminal resistance [ohms]	0.366	0.9	0.33	0.52	0.82
continuous stall [oz-in]	54.3	36	52	53	53
intermittent estimate [oz-in]	116	73	95	90	90

	BN23-28MG-03	BN23-13EU-01	BS23-28hp-03	BN28-29AF-02	BN28-21AF-01
No load speed [RPM]	8100	12200	3900	90500	9500
Kt (torque constant) [Nm/amp]	0.055	0.018	0.116	0.0491	0.0229
Torque Gradient [rpm/oz-in]	40.2	250	5.4	25	47
Power Rating [Watts]	222	91	148	263.3	210.33
Current Rating [Amps]	5.85	5.8	3.6	6.33	10.26
Voltage [V]	48	24	48	48	24
Cont/Intermittent [rpm/oz-in]	-	-	-	-	(31, 9000)
Intermittent [rpm/oz-in]	-	-	-	-	(70, 8200)
Terminal resistance [ohms]	0.576	0.465	1.06	0.25	0.14
continuous stall [oz-in]	53.2	14.6	70	74	43
intermittent estimate [oz-in]	111	33.3	125	100	75

	01500-A00	01504-A00	BN28-29AF-01	Maxon 429271	Maxon 429271
No load speed [RPM]	2340	1070	9000	3120	2080
Kt (torque constant) [Nm/amp]	-	0.2076228	0.0246	0.109	0.217
Torque Gradient [rpm/oz-in]	11.14285714	1.038834951	25	1.26351792	1.38001248
Power Rating [Watts]	29.9	-	262.4	-	-
Current Rating [Amps]	5.9	-	12.67	-	-
Voltage [V]	24	24	24	24	24
Cont/Intermittent [rpm/oz-in]	-	-	-	-	-
Intermittent [rpm/oz-in]	-	-	-	-	-
Terminal resistance [ohms]	4.1	1.8	0.087	0.522	2.28
continuous stall [oz-in]	28	109	71	79.3072	79.3072
intermittent estimate [oz-in]	56	218	100	158.6144	158.6144

Table 2 Continued

	BN23-28hp-01	BN34HS-25AF-02	BN34HS-35AF-03	BN23HS-28HS-02	maxon ECi40- 488607
No load speed [RPM]	3100	16000	10800	15800	5000
Kt (torque constant) [Nm/amp]	0.071	0.0297	0.0877	0.0219	0.091
Torque Gradient [rpm/oz-in]	5.7	55.8	16.8	26.8	3.4649664
Power Rating [Watts]	120	381	591	232	-
Current Rating [Amps]	6.1	8.6	6.5	7.3	-
Voltage [V]	48	50	100	36	48
Cont/Intermittent [rpm/oz-in]	-	-	-	-	-
Intermittent [rpm/oz-in]	-	-	-	-	-
Terminal resistance [ohms]	0.43	0.242	0.638	0.19	1.01
continuous stall [oz-in]	68	49	99	32	31.437864
intermittent estimate [oz-in]	132	78	180	55	62.875728

All of the operation points for the selected motor (Maxon 429271) and a gear ratio of 120 are shown below.

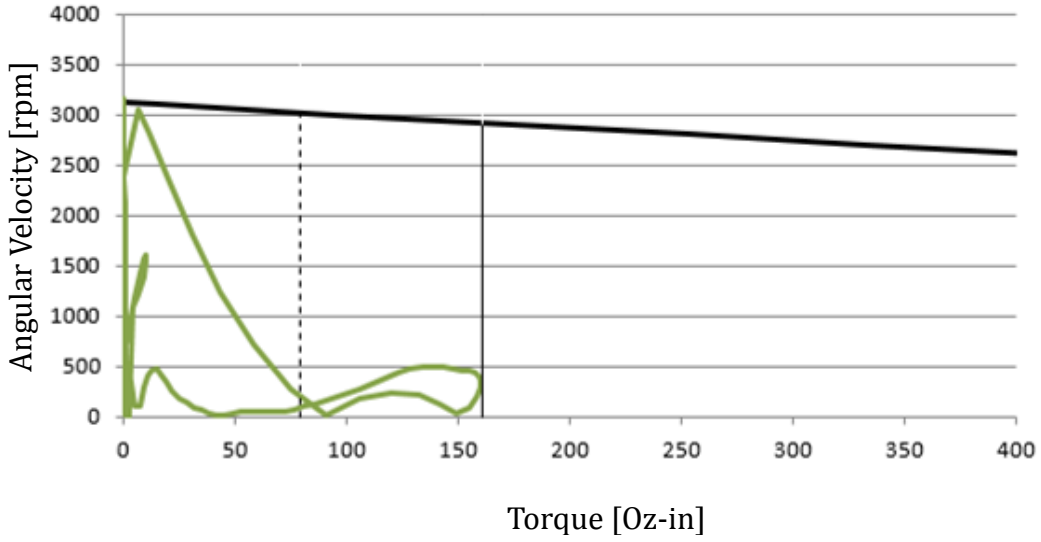

Figure 64. Operating Points for Maxon 429271

APPENDIX B: FEA DETAILS

Meshing

The mesh used for components in the bottom frame assembly that have not been described in the main paper are shown below. Shown in Figure 65, the off-the-shelf parts in the ankle are only modeled to transfer the force between the structural components. The performance of these parts in the analysis is not important so a default auto-mesh has been used.

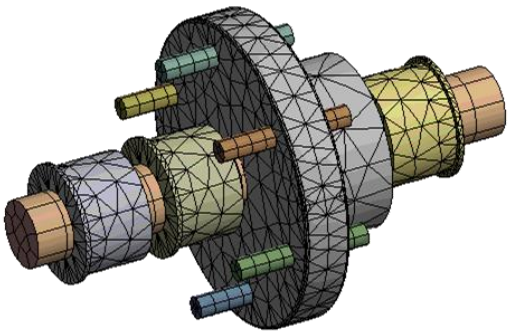

Figure 65. Mesh for Simplified Connection Parts

Connections

The following interfaces from Figure 66 and Figure 67 are perfectly bonded. Stiffness is set to update each iteration.

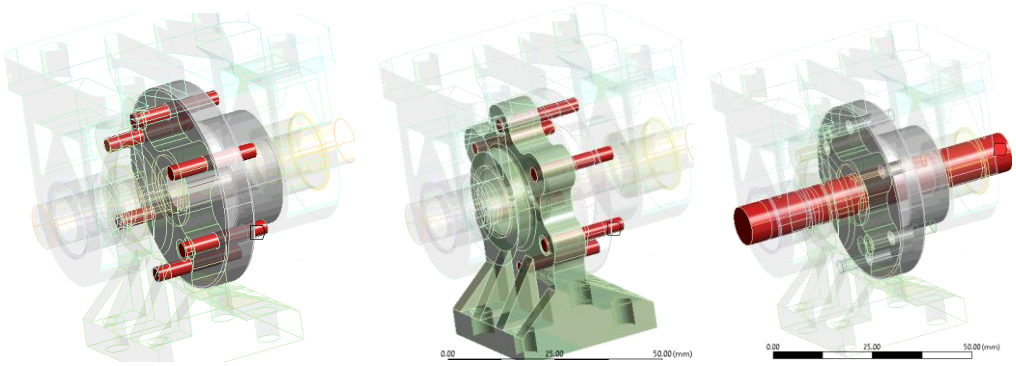

Figure 66. Ankle Interface Conditions 1

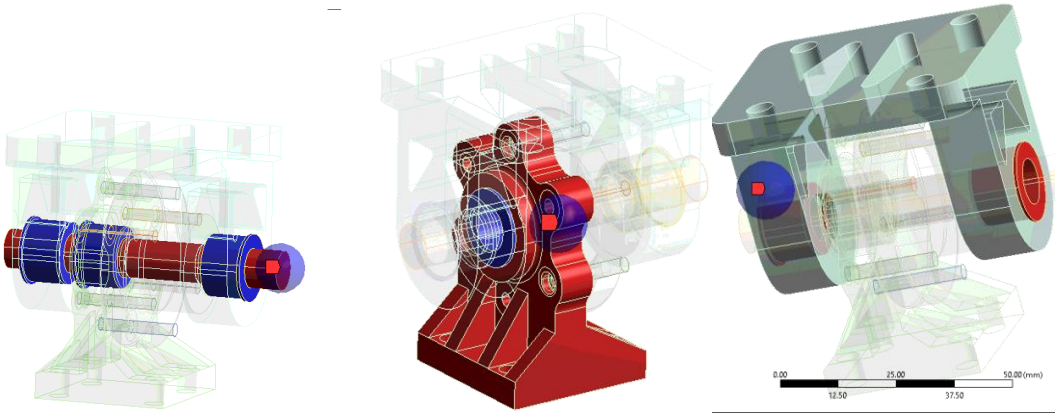

Figure 67. Ankle Interface Conditions 2

The connection in Figure 68 is a frictional displacement.

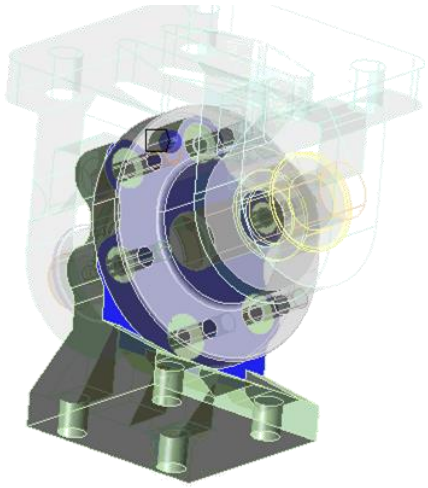

Figure 68. Frictional Interface on Ankle Bracket

Geometry design iterations:

All structural designs started by making large flat mounting plates with holes aligned for components. Unnecessary material was then removed to come to the initial designs. Iterations involved the FEA analysis runs to improve the design. The design iterations for the upper frame are shown in the figures following. The images show the geometry state (left), static structural von-Mises result (center) and fatigue safety factor (right).

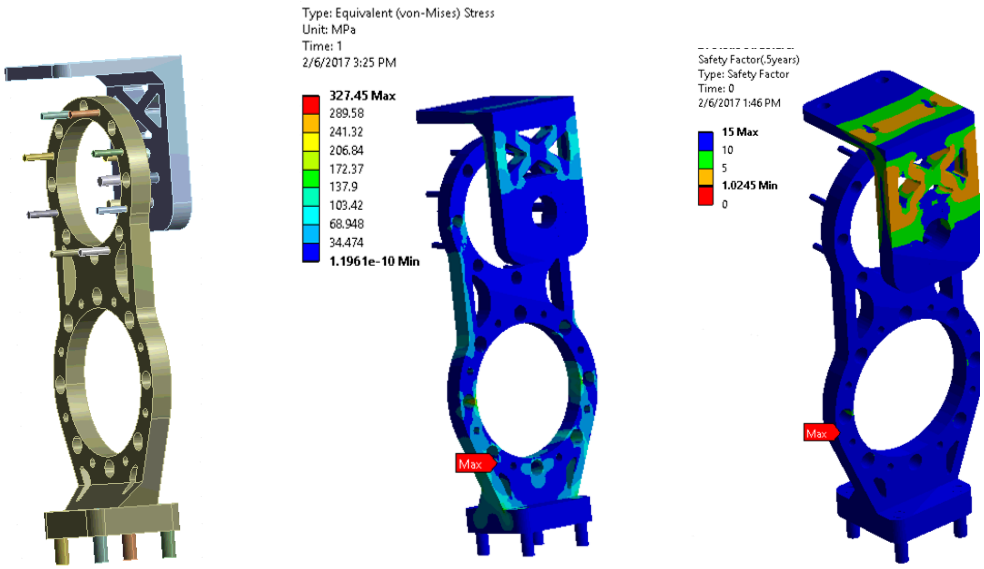

Figure 69. Top Frame Iteration 1 Results

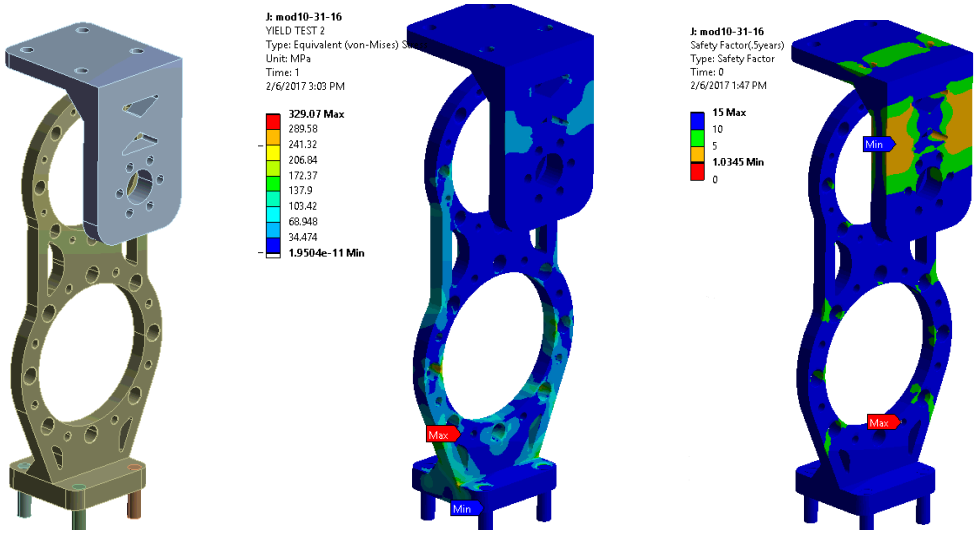

Figure 70. Top Frame Iteration 2 Results

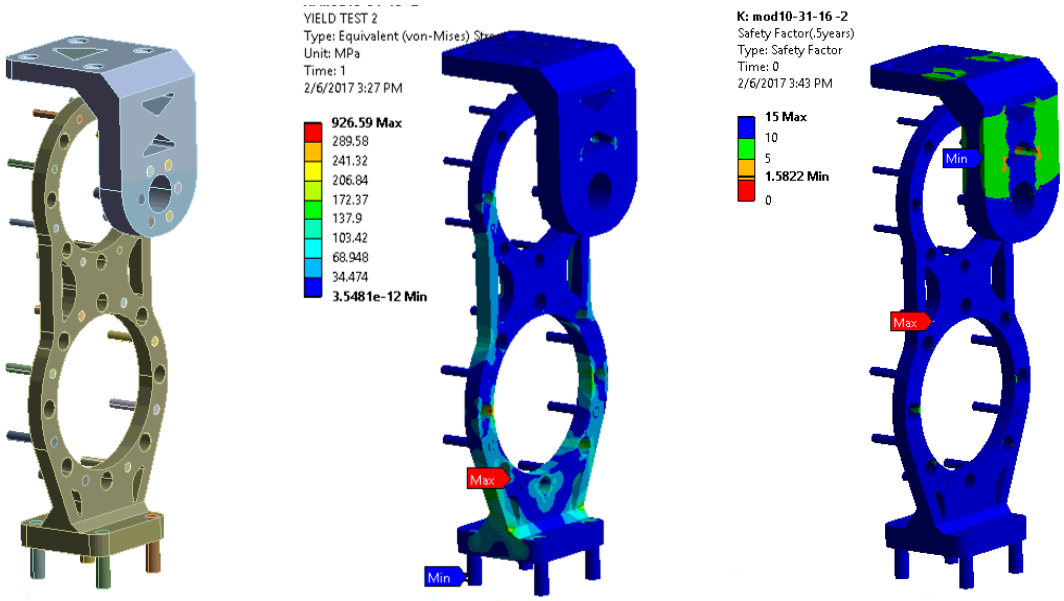

Figure 71. Top Frame Iteration 3 Results

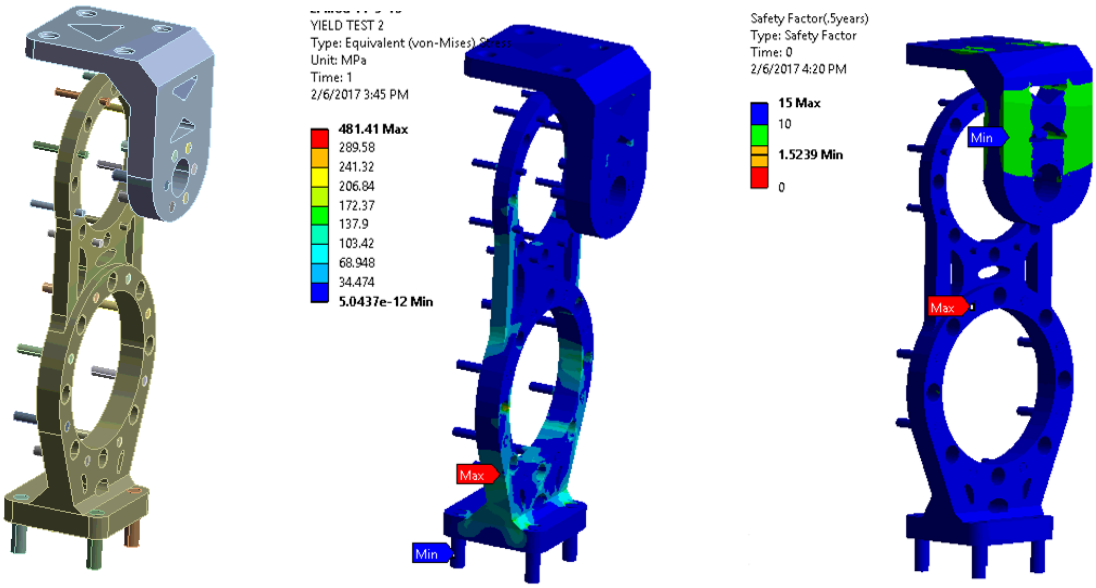

Figure 72. Top Frame Iteration 4 Results

The design iterations for the lower frame are shown in the figures below. The images show the geometry state (left), static structural von-Mises result (center) and fatigue safety factor (right).

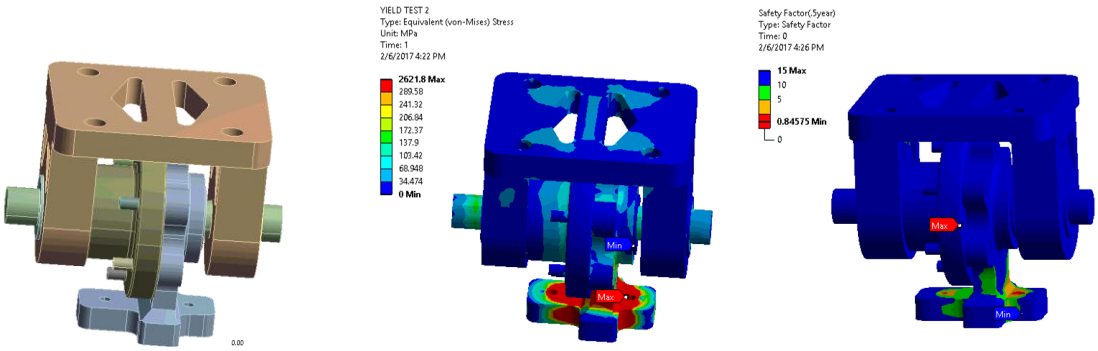

Figure 73. Bottom Frame Iteration 1 Results

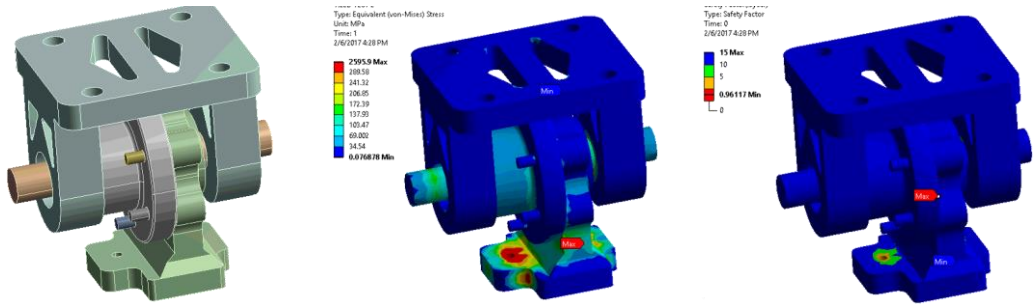

Figure 74. Bottom Frame Iteration 2 Results

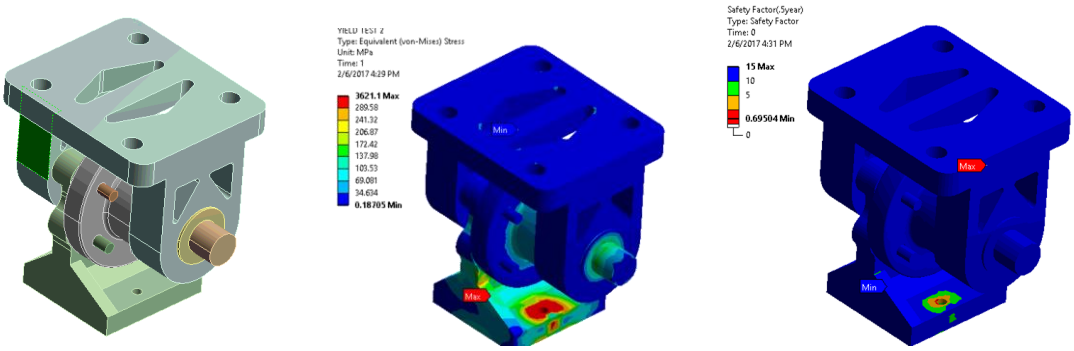

Figure 75. Bottom Frame Iteration 3 Results

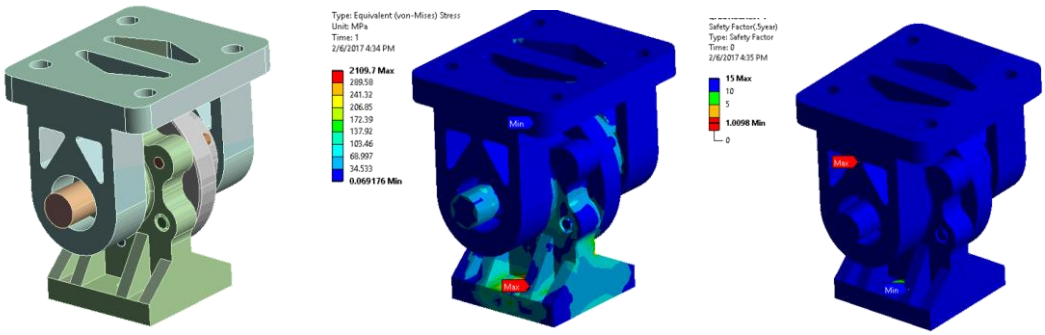

Figure 76. Bottom Frame Iteration 4 Results

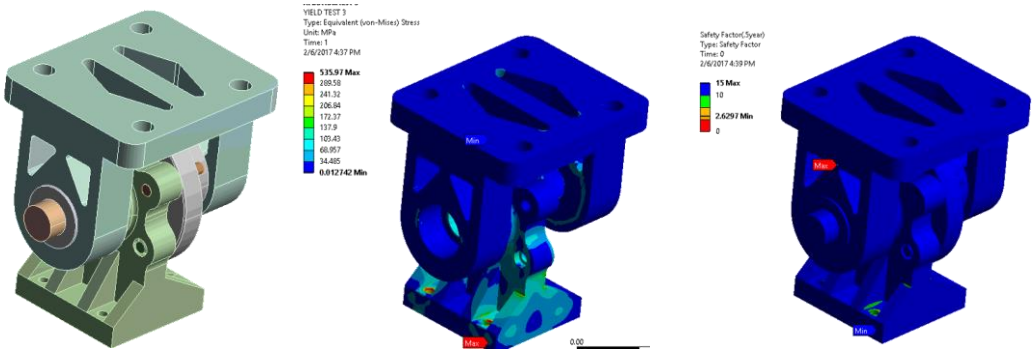

Figure 77. Bottom Frame Iteration 5 Results

The design iterations for the RSEA have been omitted due to the magnitude of iterations, which includes over 100 different designs. Design concepts that have been iterated are described in the structural section.

APPENDIX C: PROTOTYPE DRAWINGS

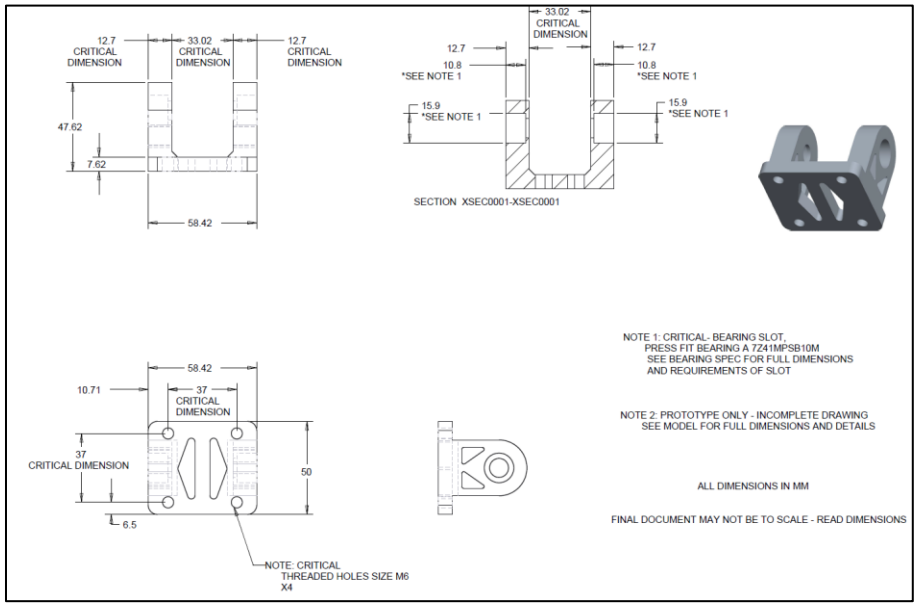

Figure 78. Ankle Link 1

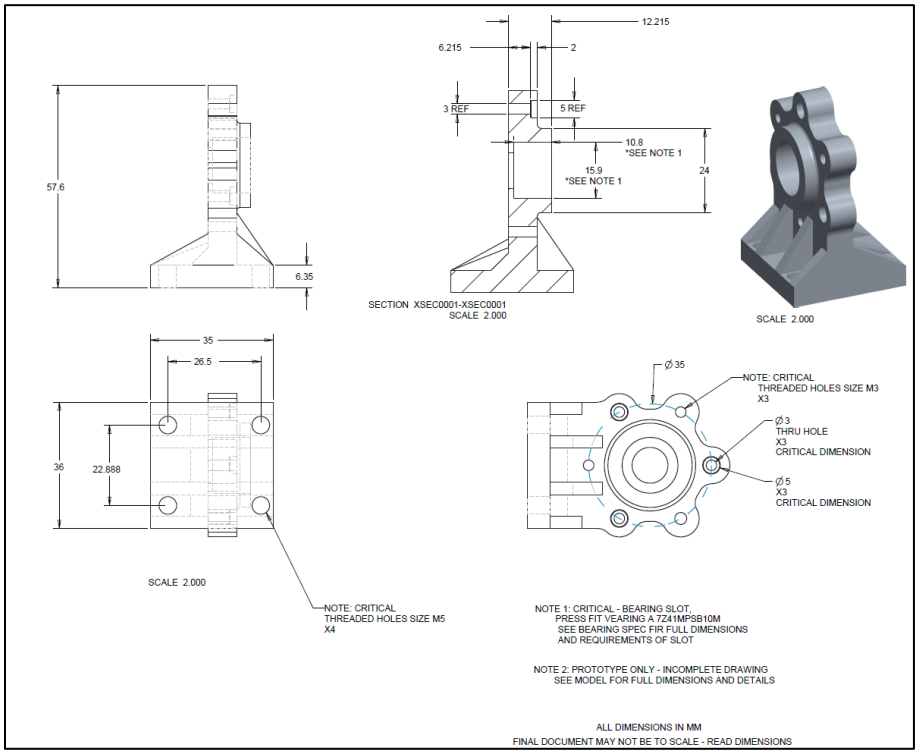

Figure 79. Ankle Link 2

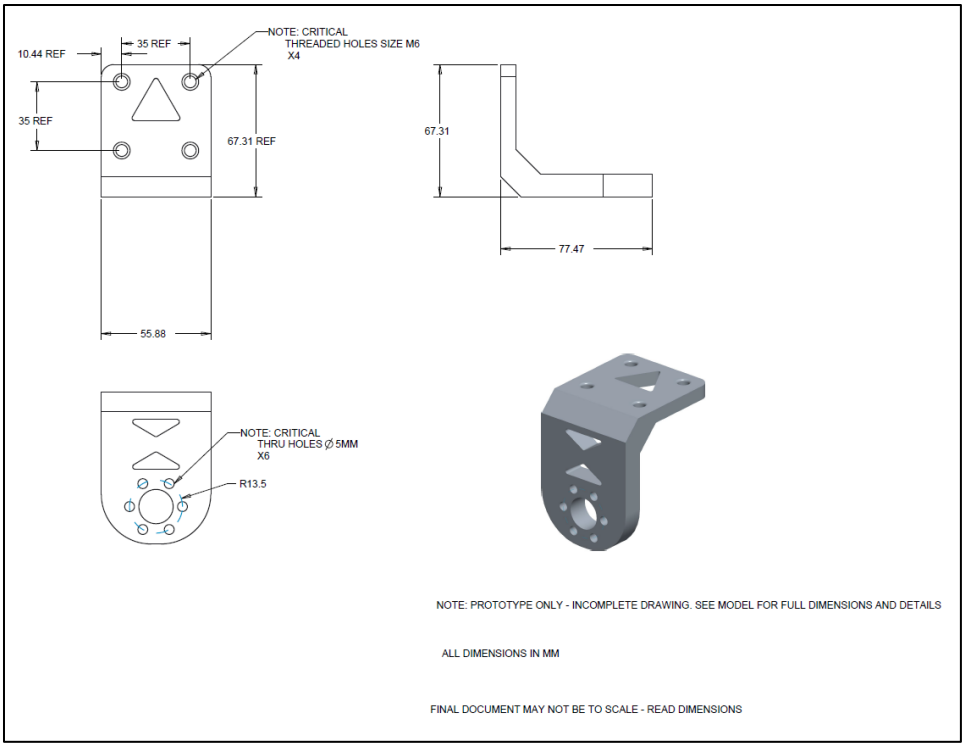

Figure 80. Top Knee

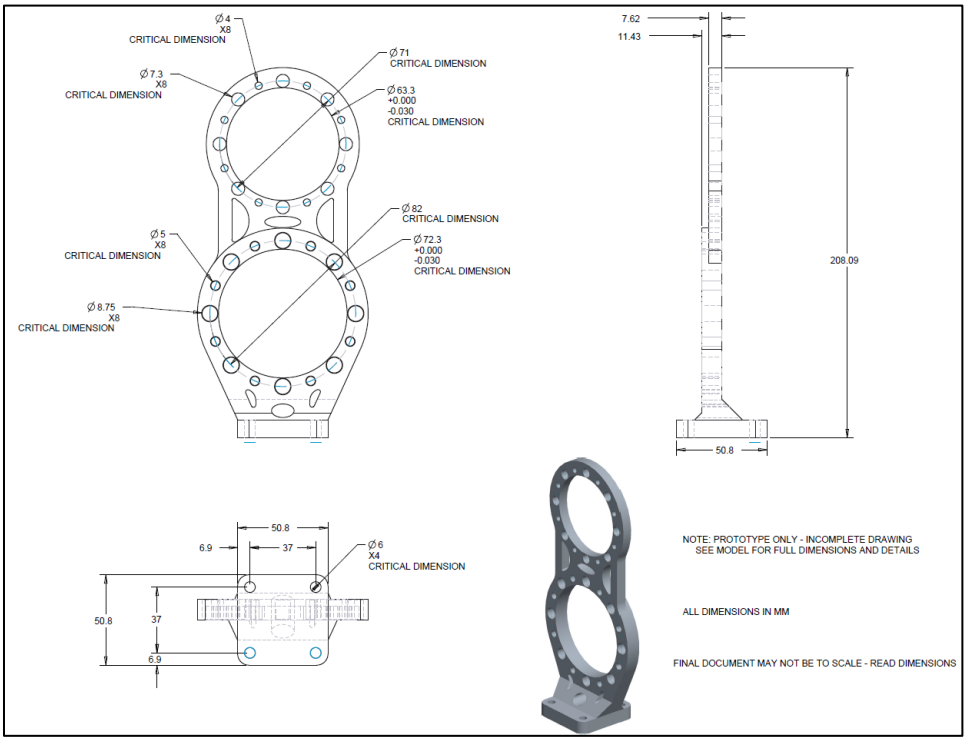

Figure 81. Top Mount